MASTERARBEIT

Titel der Masterarbeit

Investigations of Intact Human Serum Albumin and Transferrin Isoforms Interacting with Anticancer Metallodrugs by Capillary Electrophoresis

verfasst von

Christian Artner, BSc

angestrebter akademischer Grad

Master of Science (MSc)

Wien, 2014

Acknowledgment

I would like to thank

O. Univ.-Prof. Dr. Dr. Bernhard K. Keppler for giving me the opportunity to write this master thesis as part of his working group.

Mag. Lindi Grabmann and Dr. Samuel Meier for their supervision, fruitful discussions, for keeping me motivated, proofreading and giving me the freedom to work independently.

the whole working group at the Institute of Inorganic Chemistry for providing such a good working atmosphere and having fun at work and particularly after work.

Mr. Leuthner for helping me to fix the CE lift.

my friends for distracting me and always having an open ear for capillary electrophoresis issues even if they had no clue what I was talking about.

my family and especially my parents for supporting me all my life and never giving up on me.

for financial support:

and Gen-Au PLACEBO – Platform Austria for ChEmical BiOlogy.

Contents

Abstract

Metal complexes for cancer treatment, *e.g.* cisplatin, are usually administered intravenously. In the bloodstream they can bind to serum proteins such as human serum albumin (HSA) and transferrin (Tf). It has been recognized that these interactions might facilitate the transport of the metallodrug to the tumor tissue and its enrichment in the tumor but may also lead to inactivation of the drug or undesirable side effects. Post-translational modifications (PTMs) occur in both albumin and transferrin which result in microheterogeneities, *i.e.* protein subpopulations, each showing different types of PTMs at different positions. Analysis of the commercially available proteins by electrospray ionization-mass spectrometry (ESI-MS) confirmed the microheterogeneity of HSA and Tf. Four species were assigned to HSA isoforms namely native, cysteinylated, glycated and a both cysteinylated and glycated form. In case of Tf, five isoforms were detected with the tetrasialo-Tf as the most abundant one. Consequently, the presence and abundance of PTMs might affect the binding of metallodrugs to nucleophilic amino acids on these proteins depending on their proximity to the PTM.

The aim of this work was to find suitable experimental conditions to simultaneously separate intact albumin and transferrin isoforms for analysis by capillary electrophoresis (CE) with UV/Vis detection or hyphenated to mass spectrometry (CE–ESI-MS).

Method development was conducted in the CE–UV mode and different polymer-based surface coatings were screened. The coatings that showed acceptable isoform separation were tested on the durability of the polymer coating. Serial electrophoretic runs were performed over 24 h for this purpose. A neutral pluronic coating based on a poly(ethylene glycol)-*block*-poly(propylene glycol)-*block*-poly(ethylene glycol) polymer that suppresses the electroosmotic flow (EOF) and two coatings based on successive multiple ionic polymer layers (SMIL) with anionic polyelectrolytes as terminal layers and reduced EOF, in comparison to a untreated fused silica capillary, were selected and further investigated for interaction experiments with cisplatin. The pluronic coating showed the best results in case of a combined isoform separation and coating stability in the CE–UV mode. Coupling the pluronic coated capillary to ESI-MS resulted in a loss of peaks in the total ion electropherogram (TIE). A SMIL coated capillary, with poly(2-acrylamido-2-methyl-1-propanesulfonic acid) as terminal anionic layer, provided a separation of HSA and Tf but isoform resolution was not achieved in the MS mode.

Kurzfassung

Metallkomplexe, welche in der Krebstherapie Einsatz finden, wie z.B. Cisplatin, werden normalerweise intravenös verabreicht. Im Blut können sie an Serumproteine wie humanes Serumalbumin (HSA) und Transferrin (Tf) binden. Diese Interaktionen können den Transport des Metallkomplexes zum und die Anreicherung im Tumorgewebe erst ermöglichen aber auch das Medikament inaktivieren oder zu unerwünschten Nebenwirkungen führen. Post-translationale Modifikationen (PTMs) treten bei Albumin wie auch bei Transferrin auf. Dies führt zu Mikroheterogenitäten, also Protein-Subpopulationen, die jeweils verschiedene Formen von PTMs an verschiedenen Positionen zeigen. Die Untersuchung von kommerziell erhältlichen Proteinen durch Elektrospray-Ionisation Massenspektrometrie (ESI-MS) hat die Mikroheterogenität von HSA und Tf bestätigt. Vier gefundene Massen konnten HSA-Isoformen zugeordnet werden, und zwar natives, cysteinyliertes, glykiertes und sowohl cysteinyliertes wie auch glykiertes HSA. Für Tf konnten fünf Massen den Isoformen zugordnet werden, wobei Tetrasialo-Tf die größte Häufigkeit aufwies. Folglich kann das Auftreten und die Häufigkeit von PTMs bei Proteinen die Bindung von Medikamenten auf Metallbasis zu nukleophilen Aminosäuren, je nach Nähe zu diesen, beeinflussen.

Im Rahmen dieser Arbeit sollten geeignete Bedingungen gefunden werden um gleichzeitig intakte Albumin- und Transferrin-Isoformen, mittels Kapillarelektrophorese (CE) mit UV/Vis-Detektion oder gekoppelt mit Massenspektrometrie (CE–ESI-MS), zu trennen.

Zur Methodenentwicklung wurden zuerst verschiede Oberflächen-Coatings auf Polymerbasis im CE–UV Modus untersucht. Jene Coatings, die akzeptable Isoformentrennung zeigten, wurden auf ihre Langlebigkeit untersucht. Dazu wurden aufeinanderfolgende elektrophoretische Läufe über 24 h durchgeführt. Ein neutrales Pluroniccoating basierend auf einem Poly(ethylenglycol)-*block*-poly(propylenglycol)-*block*-poly(ethylenglycol)-Polymer, das den elektroosmotischen Fluss (EOF) unterdrückt, und zwei Coatings basierend auf successive multiple ionic polymer layer (SMIL), mit anionischen Polyelektrolyten als abschließende Schicht und reduziertem EOF im Vergleich zur unbehandelten Quarzkapillare, wurden in Interaktionsexperimenten mit Cisplatin getestet. Das Pluroniccoating zeigte das beste Gesamtergebnis in Bezug auf Isoformentrennung und Coatingstabilität im CE–UV Modus. Bei einer Kopplung der Pluronickapillare mit ESI-MS konnte jedoch kein Peak im Gesamtionenstromelektropherogramm registriert werden. Mit einer SMIL Coating Kapillare, bei der Poly(2-acrylamido-2-methyl-1-propansulfonsäure) die abschließende Schicht bildet, konnten HSA und Tf getrennt werden, aber jegliche Isoformentrennung verschwand.

Abbreviations

(k)Da	(kilo)Dalton (g/mol)
(k)V	(kilo)volt
(m)bar	(milli)bar
(m)Pa	(milli)pascal
(m/µ/n)M	(milli/micro/nano)molar (mmol/L; µmol/L; nmol/L)
$\Delta\mu$	migration mobility difference of two analytes
ΔP	injection pressure
°C	degree Celsius
$\bar{\mu}$	mean electrophoretic mobility of two analytes
μ_{EOF}	mobility of the EOF
μ_{HSA}	migration mobility of HSA
μ_{Tf}	migration mobility of Tf
2D	two dimensional
3D	three dimensional
A	alanine
Å	angstrom (0.1 nm)
approx.	approximately
Arg	arginine
Asn, N	asparagine
Asp, D	aspartic acid
BGE	background electrolyte
CDT	carbohydrate-deficient-transferrin
CE	capillary electrophoresis
cf.	*confer* (compare)
Cys	cysteine
CZE	capillary zone electrophoresis
D	mean diffusion coefficient
DDS	dichlorodimethylsilane
DS	dextran sulfate
e.g.	*exempli gratia* (for example)
EDTA	ethylendiaminetetraacetic acid
EIE	extracted-ion electropherogram
en	ethylenediamine
EOF	electroosmotic flow
EPR	enhanced permeability and retention effect
ESI	electrospray ionization
et. al.	*et alii* (and others)
Gal	galactose
GlcNAc	*N*-acetylglucoseamine
Glu	glutamic acid
Gly, G	glycine
h	hour
HEPES	4-(2-hydroxyethyl)-1-piperazine-ethane-sulfonicacid
His	histidine
HMA	human mercapt albumin
HNA	human nonmercapt albumin
HPC	hydroxypropyl cellulose
HPLC	high performance liquid chromatography
HSA	human serum albumin
i.d.	inner capillary diameter
i.e.	*id est* (that is)
Ile	isoleucine

L	total capillary length
Leu, L	leucine
Lys	lysine
m/z	*mass-to-charge* ratio
Man	mannose
MES	2-(*N*-morpholino)ethanesulfonic acid
Met	methionine
min	minute
M_n	number average molecular weight
M_r	relative molecular weight
MS	mass spectrometry
m_{theor}	theoretical mass
M_w	weight average molecular weight
Neu5Ac	*N*-acetylneuraminic acid
NMR	nuclear magnetic resonance spectroscopy
PAGE	polyacrylamide gel electrophoresis
PAMPS	poly(2-acrylamido-2-methyl-1-propanesulfonic acid)
PDADMAC	poly(diallyldimethylammonium chloride)
PDB	protein data bank (www.pdb.org)
PEG-PPG-PEG	poly(ethylene glycol)-*block*-poly(propylene glycol)-*block*-poly(ethylene glycol) (Pluronic F-108)
pI	isoelectric point
Polybrene	hexadimethrine bromide
PTM	post-translational modification
Q	glutamine
R	resolution
RSD	relative standard deviation
RT	room temperature
SDS	sodium dodecyl sulfate
SEC	size exclusion chromatography
Ser, S	serine
SMIL	successive multiple ionic polymer layers
t_D	migration time to the detector of analytes
Tf	transferrin
TfR	transferrin receptor
Thr	threonine
TIE	total ion current electropherogram
t_{inj}	injection time
TOF	time-of-flight
Trp	tryptophan
Tyr	tyrosine
UV	ultraviolet
V	separation voltage
V_{inj}	volume of injected sample
Vis	visible
w/v	volume percent (weight/volume)
w/w	mass fraction (weight/weight)
w_i	injection plug width
w_i^{max}	maximum injection plug width
X	any proteinogenic amino acid accept proline, serine and threonine
z	charge
ζ	zeta
η	viscosity

1 Introduction

After the discovery of the cytotoxic properties of cisplatin by Barnett Rosenberg in the 1960ies, three platinum based anticancer drugs were successfully developed for the treatment of several cancer types and are nowadays used in every second anticancer treatment worldwide (Figure 1). However, acquired resistance of some tumor cells during the treatment and severe side effects, *e.g.* nephrotoxicity and ototoxicity, overshadow the tremendous success of these metallodrugs. These limitations drive current research to develop novel anticancer drugs with different mechanisms of action and shifted the focus to alternative oxidation states or other metal centers. Currently, besides platinum there are metal-based anticancer therapeutics in clinical trials or approved for clinical use based on arsenic, ruthenium, gallium, molybdenum and gold [1].
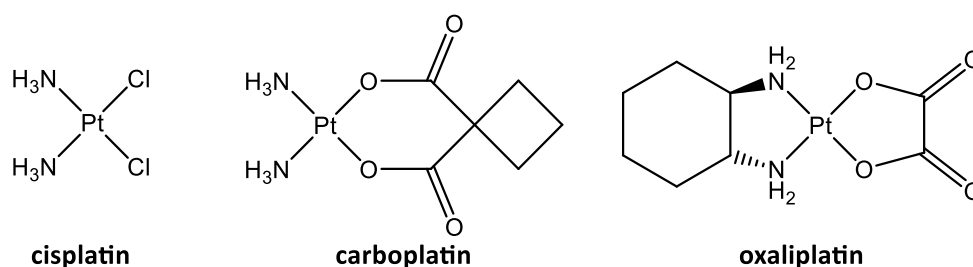

Figure 1 Structures of platinum anticancer drugs with worldwide approval.

Since metal-based anticancer drugs are generally administered intravenously, plasma proteins are among the first potential binding targets. On the one hand, this interaction may lead to inactivation of the drug or be responsible for some of the severe side effects during anticancer treatment [2]. On the other hand, the metallodrug protein binding has favorable effects, *e.g.* the enrichment of the drug in the tumor tissue due to the sustained proliferation of cancer cells or by the enhanced permeability and retention effect [3, 4]. About 90% of plasma proteins are made up by only 10 proteins. Albumin accounts for the major part with over 50% followed by the immunoglobulins G and transferrin. Importantly, albumin and transferrin are present in the plasma in various isoforms stemming from post-translational modifications (PTMs).

Until now, X-ray diffractometry and NMR spectroscopy are the primary analytical tools to characterize protein-ligand interactions on a molecular level [5, 6]. However, the downside of these methods is that they require a high amount of sample and still need subsequent purification of the protein isoforms. In addition, X-ray diffractometry only shows interactions in solid state that is not necessarily transferable to in-solution processes.

Capillary electrophoresis (CE) hyphenated to UV/Vis detection or high resolution mass spectrometry (MS) might be a powerful tool to first separate and identify protein isoforms and second, characterize metallodrug to these isoforms. In difference to other methods to separate protein isoforms (*e.g.* SEC [7], HPLC [8-12] and 2D SDS PAGE [13]) capillary electrophoresis gives the opportunity to study protein metallodrug interactions under near physiological conditions with respect to aqueous solution, buffer composition (salt concentration) and pH. These conditions are crucial maintaining the protein tertiary structure and this is especially important for protein/drug interaction experiments. A denatured protein would bring parts of the amino acid sequence to the surface which are hidden inside the protein in its native form and misleadingly reveal them as a possible interaction site. The coupling to high resolution mass spectrometry would enable to characterize the interaction products by the *mass-to-charge* ratio and further improve the limitations of CE–UV/Vis in terms of analytical selectivity and sensitivity.

Albumin and transferrin were chosen for the present study because of their high abundance in the serum and their molecular mass (<100 kDa) that enable MS measurements. Despite their average molecular masses of 66.4 kDa and 79.5 kDa for albumin and transferrin, respectively, it is possible to detect a minor mass change in the mass spectrum when a small molecule, *e.g.* a metallodrug, is added to the highly charged protein molecule ion. The molecular masses of immunoglobulins (150–950 kDa) and fibrinogen (340 kDa) do not allow to detect such small deviations in mass.

The aim of the project was the separation of intact human serum albumin and transferrin isoforms by capillary electrophoresis under electrospray ionization-mass spectrometry (ESI-MS) compatible conditions to investigate the binding of anticancer metal complexes to these isoforms.

2 Blood

The human blood supplies oxygen, nutrients and drugs to the cells of the body and carries metabolic waste products away from them. It has a distinct pH of 7.4. The approximately 5 liter of blood in healthy adults are composed of the blood plasma and different types of cells, namely erythrocytes, leukocytes and thrombocytes [14].

The blood plasma is an aqueous solution containing many different dissolved compounds such as nutrients, hormones, waste products, electrolytes and proteins (*e.g.* albumin and transferrin). When plasma is extracted from whole blood, an anticoagulant (*e.g.* EDTA or citric acid) is added and centrifugation divides the cells from the plasma. Blood serum does not require an anticoagulant, but the blood clogs and the clotting factors (mostly fibrinogen) are separated by centrifugation from the liquid part together with the blood cells. Therefore, blood serum is basically blood plasma without fibrinogen. Table 1 gives an overview of important components in the serum [15, 16]. The total protein amount in serum of healthy adults is 63–82 g/L [15].

Table 1 Main constituents of human blood [15, 16]. All values refer to serum if not otherwise indicated.

Compound	Concentration ranges [mmol/L]
Na^+	137–145
Cl^-	98–107
HCO_3^-	22–30
Glucose (fasting, plasma)	4.1–6.0
K^+	3.6–5.0
Urea	2.5–7.5
Ca^{2+}	2.10–2.55
PO_4^{2-}	0.8–1.45
Lactate (whole blood)	0.7–2.1
Mg^{2+}	0.70–1.00
Albumin	0.530–0.750
Immunoglobulin G	0.040–0.100
Zn^{II}	0.011–0.024
Cu^{II}	0.011–0.022
Transferrin	0.025–0.045
$Fe^{II/III}$	0.0066–0.0324
Fibrinogen (plasma)	0.0059–0.0106
Immunoglobulin A	0.005–0.025
Bilirubin	0.003–0.022
Immunoglobulin M	0.0005–0.002

2.1 Albumin

The most abundant protein in human blood is serum albumin (HSA). It preserves the oncotic pressure and acts as a modulator of fluid distribution between body compartments. HSA is encoded by the single copy gene ALB which is located on chromosome 4. First, the single chain protein is synthesized in the cytosol of hepatocytes. After translation the pre-pro-albumin is modified into pro-albumin in the lumen of the endoplasmatic reticulum. Further, furin cleaves a 6-amino-acid sequence at the *N*-terminus in order to obtain the mature and unmodified protein, consisting of 585 amino acids and a molecular weight of 66438 Da (Figure 2) [17]. In this state it is released to the blood stream. HSA has a long life-time of 28-36 days where it can undergo several PTMs that might affect ligand binding and anti-oxidant properties [18].
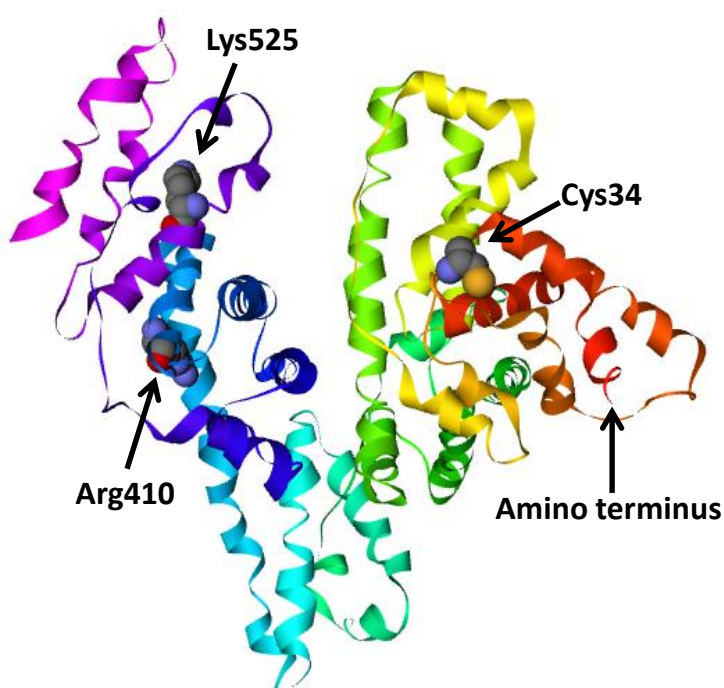

Figure 2 The 3D structure of human serum albumin (PDB 4G03). The major sites for modification are accentuated. The *N*- and *C*-termini are colored red and magenta, respectively.

Albumin contains only one tryptophan, the content of Met, Gly and Ile residues is low, while Cys, Leu, Glu and Lys are frequent. The large number of ionized residues causes a high total charge (215 ions per HSA at pH 7.0) that accounts for its good water solubility. There are more acidic than basic residues resulting in a negative net charge at pH 7 of approximately -15 per protein. The 35 Cys residues build 17 disulfide bridges, causing stability and a long biological life-time. The remaining free cysteine is at position 34 [17]. The secondary structure contains exclusively α-helices (68%). The globular conformation is heart-shaped with approximate dimensions of 80 x

80 x 30 Å [19]. The serum concentration of HSA is approx. 600 µM in healthy individuals. The concentration decreases slightly during pregnancy, together with other serum proteins, and drastically in individuals suffering from analbuminemia, a rare recessive disorder. Monitoring the HSA value is also an important indicator for progression in certain diseases including cancer, rheumatoid arthritis, ischemia or post-menopausal obesity [18].

2.1.1 Modifications of albumin

The structure of albumin is not consistent despite being translated from a single copy gene. HSA has a microheterogeneity due to PTMs that may alter its redox and binding properties to endogenous as well as exogenous substances, including anticancer drugs.

In healthy adults, 70–80% of HSA molecules have a free Cys34 residue. It provides the largest pool of free thiol in the human serum. Approximately 25–30% of these Cys34 form disulfide bridges mostly with cysteine, but also with homocysteine or glutathione [20].

The main targets for *N*-homocysteinylation are the lysine residues 4, 12 and 525. In healthy individuals about 0.26–0.36% of the circulating HSA is *N*-homocysteinylated. Increased values are associated with cardiovascular and neurodegenerative disorders such as dementia and Alzheimer´s disease [21].

The characteristic Asn-X-Ser/Thr sequence for *N*-glycosylation is absent in the primary structure of HSA and, therefore, HSA is not a glycoprotein. Nevertheless, HSA can undergo glycation, a non-enzymatic reaction with a monosaccharide [22]. The major sites for this modification are Arg410 and Lys525 while minor sites are Arg114, Lys186, Lys199, Arg218, Lys281, Arg428 and Lys439 [23, 24]. The glycation influences the protein conformation and the binding properties of different ligands such as warfarin, bilirubin, fatty acids, Cu(II) or Fe(III) [20, 25-27]. Usually, about 10% of HSA is glycated, but this level is increased to 20–30% in hyperglycemic individuals [28].

HSA is able to store and transfer NO [18, 29]. About 82% of the NO in the blood is bound to the Cys34 residue of HSA [17]. HSA can also bind NO at Trp and Tyr residues. Cys34 nitrosylation reduces the HSA binding affinity of Cu(II) ions, phenolsulfophthalein, and palmitic acid allosterically [30].

Oxidation of serum proteins by reactive oxygen species is more common in elderly than in young individuals. Oxidative stress can activate inflammatory pathways leading to a transformation of a normal cell into a tumor cell. Consequently, oxidation may be associated with cancer [31]. The

most prominent targets for oxidation are Cys34 and Met residues [11]. Since these residues are known to act as metal chelators [32] oxidation may decrease the binding properties to metal based anticancer drugs.

Turell *et al.* recently applied an anion exchange HPLC column for separating HSA isoforms based on their isoelectric point (pI). They reported a pI for native HSA of 4.88 ± 0.06, 4.78 ± 0.06 for the oxidized form HSA-SO$_2^-$ and for HSA with mixed disulfides a pI between these two values [10].

2.1.2 Albumin metal binding sites

To this point, three major metal binding sites have been identified: the *N*-terminal binding site [33], the free Cys34 [17] and the so-called primary multimetal binding site where His67, Asn99, His247 and Asp249 are involved [34]. Some metal ions might also bind to the protein either unspecifically or to yet undefined regions [17].

2.1.2.1 N-terminal binding site

The *N*-terminal binding site is the first metal binding site that was identified. It is the primary binding site for Cu(II) and Ni(II). These two metal ions can be chelated by the *N*α atom of Asp1, the deprotonated *N*α of Ala2 and His3, and the *N*δ of His3 in a square planar geometry [33, 35]. In the binding of Co(II) two additional groups, the β-COO$^-$ group of Asp1 and the *N*ε of Lys4, are involved as axial ligands in an octahedral arrangement [18, 33]. Experimental data suggest that the first two amino acids at the *N*-terminus are cleaved off in approx. 25% of circulating HSA. Interestingly, this loss of amino acids is unique to humans and was not found in other mammalian serum [36]. The degradation might lead to an altered affinity for metal ions at the *N*-terminal binding site.

2.1.2.2 Cys34 binding site

The free Cys34 thiol group is located inside a cleft. Therefore, access is narrowed and results in higher specificity for metal ion interactions [35]. The special structure of the Cys34 binding site is responsible for the distinct binding to Au(I) and Pt(II) (*e.g.* from cisplatin) [35, 37-39]. Ag(I) [40] and Hg(II) [41] are also likely to bind to this thiol with high affinity. Experiments based on nuclear magnetic resonance and site-directed mutagenesis indicate, that Cd(II) and Zn(II) are excepted from binding to Cys34 [42] (see next paragraph).

2.1.2.3 Multimetal binding site

The multimetal binding site has high affinities to Cu(II), Ni(II), and Zn(II) with dissociation equilibrium constants in the μM range, and Cd(II) with a dissociation equilibrium constant larger by an order of magnitude [43, 44]. Approx. 98% of plasma Zn(II) is bound to HSA serving as the major carrier for Zn(II) in the human plasma [17, 34, 45]. The multimetal binding site acts as the primary binding site for Cd(II) [46] while it is the secondary target for Cu(II) (and possibly Ni(II)) with the *N*-terminal site being the preferential one [47, 48]. The binding of fatty acids to HSA can provoke allosteric effects where the two domains containing the residues (His67, Asn99 and His247, Asp249) involved in metal binding in the multimetal binding site become spatially divided. Thus, fatty acids (and possibly also other small molecules) might affect the transport and delivery of metal ions (especially Zn(II)) in the blood [34, 42].

2.1.2.4 Platinum binding sites

Invanov *et. al* investigated reactions of cisplatin with albumin using 15N labeled cisplatin in combination with two-dimensional 1H,15N NMR spectroscopy, natural and recombinant HSA and chemical modifications of Cys, Met and His residues. Their data suggests that cisplatin mainly binds bifunctionally to *S,N*-Met. Met298 might be the major binding target as it seems to be the most surface accessible Met residue based on crystal structure data of HSA. Minor binding sites are of a monofunctional type involving *S*-Met and Cys34 [38].

2.1.3 Albumin in cancer

Solid tumors are able to trap plasma proteins and use their degradation products for proliferation and growing [49]. The high abundance of HSA in the blood makes it the major energy and nutrition source for highly metabolically active cancer cells. Due to the fast growth of tumors the surrounding vascular system becomes leaky. HSA with a diameter of approx. 8 nm is, therefore, able to enter the microenvironment of the tumor. The higher permeability of tumors affects smaller molecules in a similar way. However, macromolecules with >40 kDa display a higher retention and enrich in the tumor tissue because of reduced clearance from the tumor tissue due to an impaired or absent lymphatic system. This is also known as the enhanced permeability and retention effect (EPR). When radiolabeled albumin is given to mice about 20% of the given dose is found accumulated in the tumor tissue. Consequently, HSA has been investigated as a delivery system for anticancer drugs to the tumor tissue [3, 4, 50].

In advanced cancer stages malnutrition and inflammation suppresses HSA synthesis, leading to a reduced concentration in the blood. As low HSA levels are associated with poor outcome in cancer patients, the HSA concentrations in the blood of patients are determined to monitor the nutritional status, the severity of the disease and the disease progression [18].

2.2 Transferrin

Transferrin (Tf) is a glycoprotein. It has an average mass of approx. 79.5 kDa and consists of 679 amino acids in a single peptide chain (Figure 3). It is the most important iron transporting protein and is capable of binding two Fe(III) ions, one in each of the two globular domains. Therefore, the 30 µM Tf in serum are divided into four species only differing in their iron content or location: iron-free Tf (apo-Tf, ~40%), monoferric C-lobe Tf (Fe$_C$Tf, ~10%), monoferric N-lobe Tf (Fe$_N$Tf, ~23%) and diferric Tf (holo-Tf, ~27%) [51]. Holo-Tf and the transferrin receptor (TfR) attached to the cell surface form a complex with nM affinity. The protein-receptor complex undergoes clathrin-mediated endocytosis. Further, Fe(III) is liberated from the Tf complex in the more acidic environment of the endosome (pH = 5.6), is then reduced to Fe(II) [52, 53] and transported to the cytoplasm. Apo-Tf and TfR also form a complex at endosomal pH that allows the return to the cell surface, where apo-Tf is released again into the blood stream [54].

The two structural similar domains of Tf, *i.e.* the C-lobe and N-lobe, are linked by a short random coil peptide chain (Figure 3). These two lobes can be further divided into two spheres with comparable size which have alternating α-helical and β-sheet sections. The two spheres create a cleft where the iron binding site is located. Fe(III) is bound in a distorted octahedral geometry with two Tyr, one His, one Asp, and a bidentate carbonate anion as ligands. The metal binding is weak without the synergistic carbonate anion from the buffer [55].
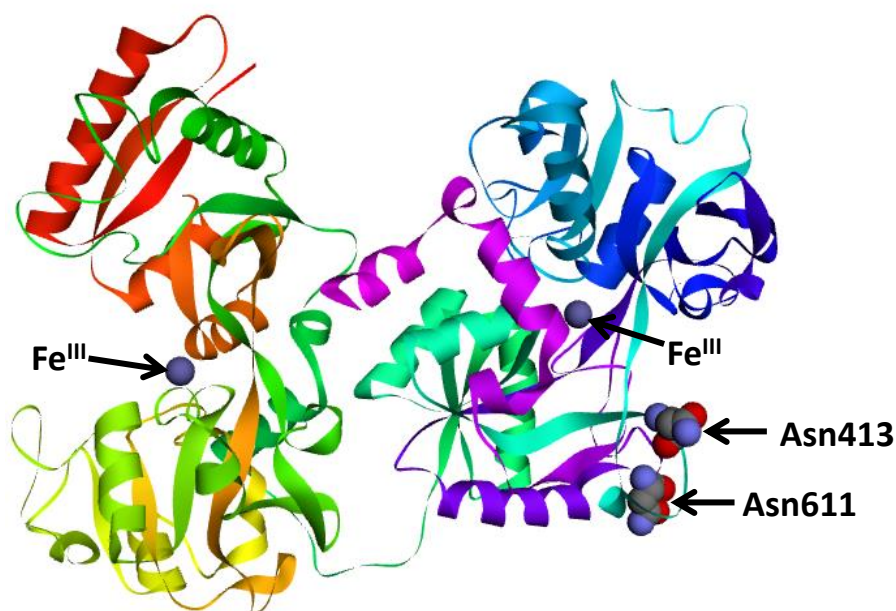

Figure 3 The 3D structure of human serum transferrin (PDB 3QYT). One Fe(III) is bound to each of the two globular domains (N-lobe and C-lobe). The two major glycosylation sites are at Asn413 and Asn611 both situated in the C-lobe. The N- and C-termini are colored red and magenta, respectively.

2.2.1 Heterogeneity of transferrin glycan structures

There are two major *N*-glycosylation sites located in the *C*-terminal domain of the protein at the Asn413 and Asn611 (Figure 3) [56], and one minor glycosylation site at Asn472 [57]. The carbohydrate chains build up with *N*-acetylglucosamine, mannose, galactose and sialic acid. A core fucosylation only occurs at Asn611. While the minor glycosylation is only occupied by the biantennary type, the glycans linked to Asn413 and Asn611 can differ in the degree of branching and in the number of sialic acids [58]. At Asn413 and Asn611 there are di-, tri-, and tetra-antennary glycan structures that are usually terminated with a sialic acid which is always *N*-acetylneuramic acid in humans (Figure 4) [59]. The sialic acid group provides a negative charge on the carboxylic acid moiety. Therefore, Tf isoforms differ in their total charge due to their different number of sialic acids. The most abundant isoform is tetrasialo-Tf [60].
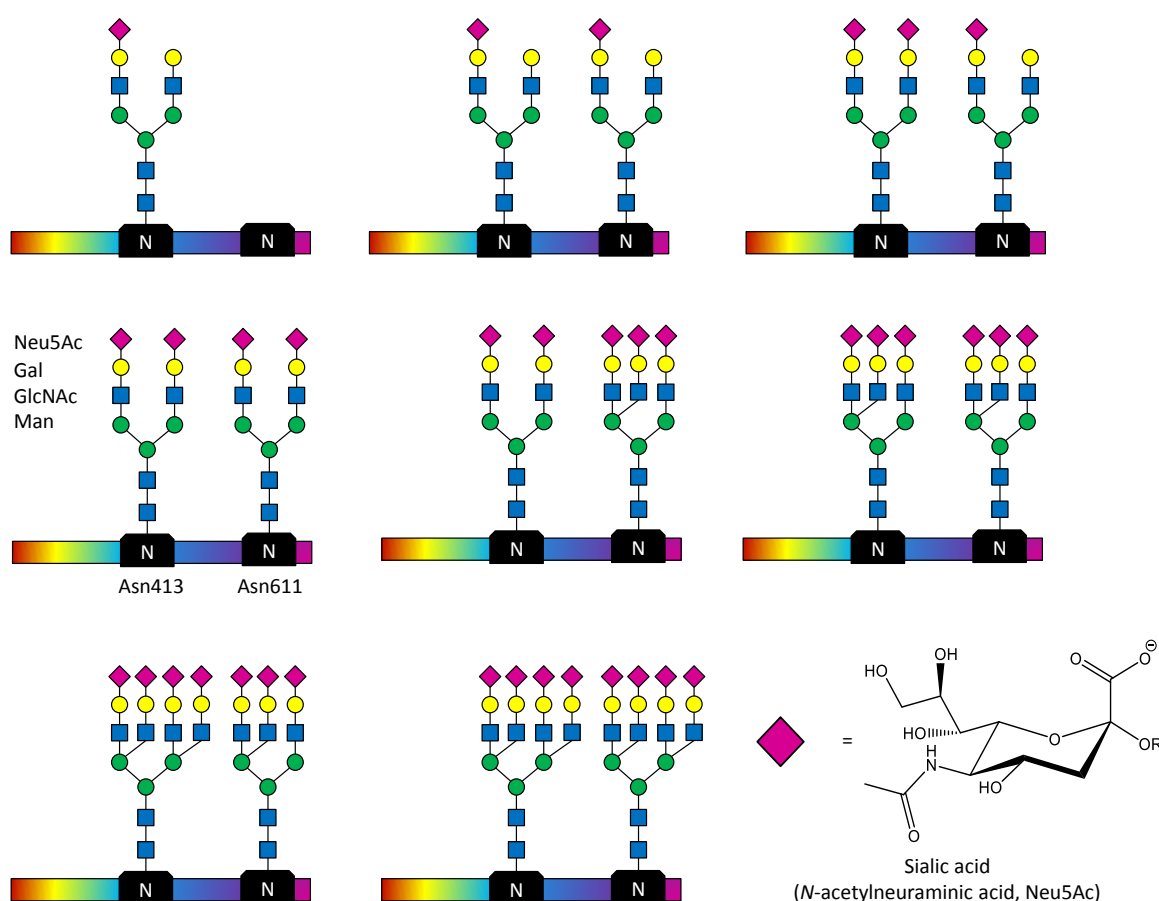
Figure 4 Examples for transferrin glycan structures. The glycan part of the protein can differ in the number of branches and sialic acid groups. The isoform with 4 terminal sialic acids is the most abundant one (Gal = Galactose, GlcNAc = *N*-acetylglucoseamine, Neu5Ac = *N*-acetylneuraminic acid, Man = Mannose).

As a result, Tf exhibits a micro-heterogeneity due to variations in carbohydrate structure, the number of sialic acid residues and iron content. The most abundant tetrasialo-Tf has an

isoelectric point (pI) of 5.4 after complete iron saturation. The Tf isoform with six sialic acids has a pI of 5.0, pentasialo-Tf 5.2, trisialo-Tf 5.6, disialo-Tf 5.7 and the asialo form 5.9 [61]. Moreover, the pI decreases by approx. 0.2 pH units for each of the two Fe(III) [62].

Experiments on the influence of the Tf glycan structures with respect to receptor binding seem to be contradictory. On the one hand, the carbohydrate chains of Tf seem to have no influence on the binding affinity to the TfR as non-glycosylated recombinant Tf was found to be functionally indistinguishable from ordinary glycosylated serum Tf [63, 64]. On the other hand, the uptake of iron and protein is lower from deglycosylated Tf. The reason for this could be a decreased endocytosis rate of aglyco-Tf. Shortening the glycan branches down to the mannose fork has the same iron uptake characteristics as the unmodified Tf. Aglyco-Tf has lower iron uptake abilities indicating that the branched mannose structure is important for iron binding abilities [65].

In certain types of non-human Tf the glycans may be responsible in stabilizing the protein in its biologically active conformation, *i.e.* the glycans of the rabbit serum transferrin are building a bridge between the two lobes of the protein. The glycan structures in human serum Tf are in an external position and seem to have no stabilizing function [66].

2.2.2 Transferrin in cancer

The blood serum in healthy adults contains Tf in a concentration of approx. 30 µM. Lower Tf serum levels are found in patients suffering from inflammation [67], ovarian cancer [68, 69] and other gynecological cancers [69]. After chemotherapeutic treatment, the Tf serum levels of ovarian cancer patients may increase [68]. Besides, glycosylation alterations are associated with certain diseases such as immune deficiency, autoimmune diseases, chronic alcoholism and cancer [70]. Under- and overexpression of certain glycans as well as an expression of glycans, normally only found in embryotic tissue (*e.g.* polysialic acid) is reported for cancer. Structural changes mostly arise from changes in the expression levels of glycosyltransferases in the Golgi apparatus of cancer cells, often resulting in an increase of branching of *N*-glycans [71]. This and overexpression of sialyltransferase results in higher extents of sialylation [72]. Additionally, patients suffering from hepatocellular cancer show increased levels of highly branched fucosylated glycans in Tf [73].

The transferrin receptor is upregulated in cells of certain cancer types. Therefore transferrin would make a suitable targeted device to deliver metal based anticancer drugs into cancer cells [74].

2.2.3 Platinum binding sites

Cox *et al.* used 13C labeled Pt(en)Cl$_2$ and 15N labeled cisplatin to study their interactions to Tf in combination with two-dimensional 1H,13C and 1H,15N NMR spectroscopy, respectively. The experimental data suggests that monodentate solvent exposed *S*-Met are the major binding sites for platination with the Met256 being the most preferred one. The monodentate interaction between *S*-Met and Pt(II) is reversible. This gives Tf the possibility to act as a delivery device for anticancer drugs. However, they only used recombinant and deglycosylated Tf for their study, what makes the role of the glycan structure still unclear [75].

Using mass spectrometric approaches, Allardyce *et al.* found the Thr457 residue of Tf to be modified by cisplatin. They incubated Tf with cisplatin, digested the mixture with trypsin and analyzed the resulting peptides by liquid chromatography/tandem mass spectrometry. They were not able to detect the peptide containing Met256. Further, finding a peptide with a platinated Thr457 does not necessarily indicate that the intact Tf is also modified at the same residue [76].

3 Capillary Electrophoresis

Capillary electrophoresis (CE) is one of the most powerful separation techniques in modern analytical chemistry as exemplified by the unraveling of the human genome [77]. CE gives the opportunity to work under near physiological conditions with respect to pH, aqueous solutions, buffer composition, and temperature. Moreover, it provides high efficiency and selectivity.

The experimental setup of a capillary zone electrophoresis (CZE) is simple (Figure 5). Two vials are filled with an aqueous background electrolyte (BGE). Each vial contains an end of a fused silica capillary and one electrode to provide an electrical contact between the high voltage power supply and the capillary. Upon the separation process the capillary is filled with the BGE using a pressure system. The sample is injected into the capillary by replacing the inlet vial with the sample vial and applying pressure for a short time. Then, the sample vial is changed back to the BGE containing vial and an electric field is applied for separation. On the opposite end of the capillary optical detection can be executed directly through the uncoated capillary wall. The outlet end can also be hyphenated to an external detector (*e.g.* mass spectrometer).
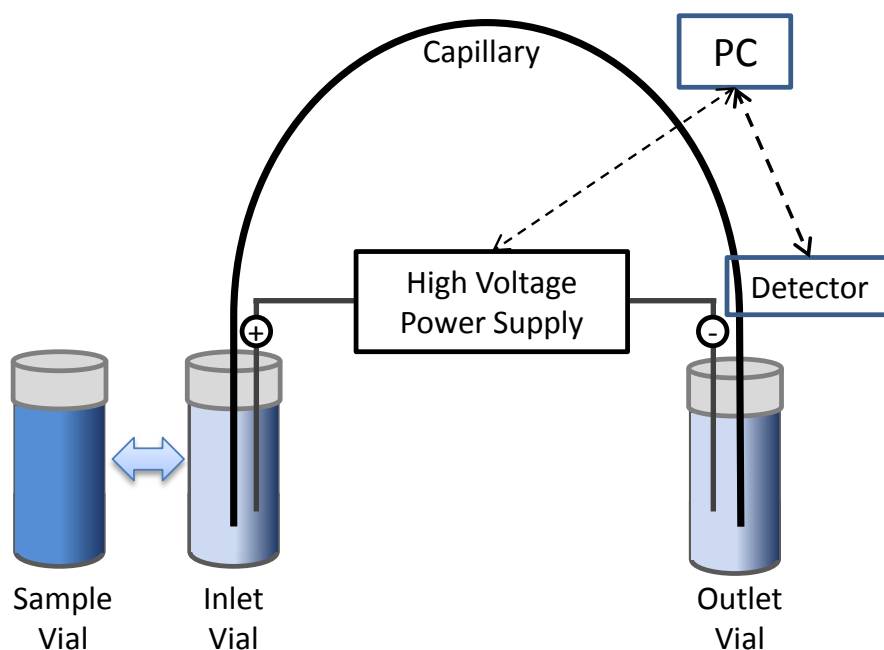
Figure 5 Basic components of a capillary electrophoresis system. Adapted from [78].

The electrophoretic separation is based on the different velocities of analytes in an electric field, which are termed mobilities. Small, highly charged species have high mobilities whereas large, lowly charged species have low mobilities resulting in the separation of species with different *charge-to-size* ratios [78].

3.1 Electroosmotic flow (EOF)

CE is usually performed in a fused silica capillary. The inner wall of the capillary is covered by silanol groups that can, depending on the pH, exist in the anionic form. Cationic counterions build up near the surface to a diffuse double-layer and create a potential difference called the ζ-(zeta) potential (Figure 6A). When a voltage is applied across the capillary, the solvated cations move toward the cathode and drag the bulk solution with them. This bulk movement is called electroosmotic flow (EOF). It has a flat flow velocity profile. This is favorable since it does not contribute to the broadening of sample zones. This is in contrast to a pressure driven (laminar) flow with a parabolic flow velocity profile, which occur during chromatographic processes (Figure 6B) [78, 79].
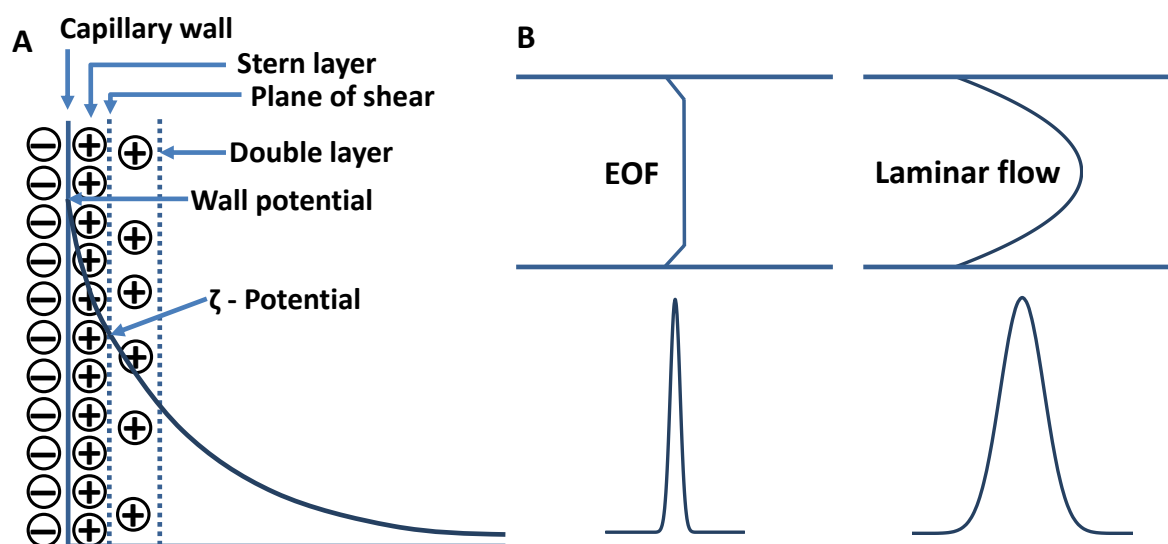
Figure 6 Electroosmotic flow. (A) Electrical double layer at the capillary wall. (B) Flow profiles and corresponding solute zones in electro- (*EOF*) and pressure (*Laminar flow*) driven flow. Adapted from [79] and [78].

Cations obtain an additional velocity in this setup, while neutral molecules co-migrate with the EOF and anions are forced in the opposite direction. The EOF is usually stronger than the different analyte mobilities leading to a transport of all molecules to the cathodic end of the capillary and to the detector. Typical flow rates are between approx. $3\text{–}8 \cdot 10^{-4}$ cm^2 V^{-1}s^{-1}. The surface charge of the capillary is pH dependent. Consequently, the extent of the EOF varies with pH. At low pH the silanol groups are protonated. Therefore, the EOF is weaker than at high pH where the silanol groups are deprotonated leading to a higher surface charge. The EOF is also

dependent on the ionic strength of the BGE. Higher ionic strength results in a compressed double layer, a lower ζ-potential and lower velocity of the EOF [78, 80].

The EOF is not only a property of silica surfaces. Other types of surfaces can be generated using chemical or physical interactions, resulting in negative, positive or neutral surfaces. These new surfaces influence the velocity or the direction of the EOF or may even suppress it [81].

3.2 Zone broadening

The separation of two sample zones is based on their difference in migration time and their sample zone width. The most important factors that contribute to sample zone broadening are longitudinal diffusion, Joule heating, electrodispersion, unleveled buffer reservoirs, the length of the injection plug (see section 3.2.1) and solute-surface interactions (see section 3.2.2).

The longitudinal diffusion defines the limit of efficiency. However, the low diffusion coefficient of proteins is beneficial for the efficiency. Joule heating leads to radial temperature gradients and parabolic flow velocity profiles. Lower inner capillary diameters are preferred to make the heat removal more efficient. The surrounding environment of the capillary should be controlled with a cooling system *e.g.* by a high velocity air circulation.

Electrodispersion is caused by mismatched conductivities of sample and BGE. Samples with higher conductivities than the running buffer lead to fronting, ones with lower conductivities result in tailing [78, 82].

3.2.1 Injection plug width

In case of hydrodynamic injection the volume of the sample loaded V_{inj} can be calculated by the Hagen-Poiseuille equation (Equation 1), which is a function of the capillary dimension (the inner capillary diameter *i.d.* and the total capillary length L) the viscosity of the BGE η, the applied pressure ΔP and time t_{inj}.

Equation 1 Hagen-Poiseuille equation. V_{inj} = volume of sample loaded, ΔP = applied pressure, *i.d.* = inner capillary diameter, t_{inj} = injection time, η = viscosity of the BGE, L = total capillary length.

$$V_{inj} = \frac{\Delta P \, (i.d.)^4 \, \pi \, t_{inj}}{128 \, \eta \, L}$$

The lengths of the injected sample plugs w_i should be narrow and not extend the standard deviation due to diffusion $(2Dt_D)^{1/2}$ to avoid loss of resolution. D is the diffusion coefficient and t_D

is the analyte migration time to the detector. When a 10% loss of resolution by injection is assumed to be acceptable, the relationship between the standard deviation due to sample injection $w_i/12^{1/2}$ and the standard deviation due to diffusion $(2Dt_D)^{1/2}$ is shown in Equation 2.

Equation 2 Relationship between the standard deviation due to sample injection and the standard deviation due to diffusion. w_i = width of the injected sample plug, D = diffusion coefficient of the analyte, t_D = migration time of the analyte to the detector.

$$\frac{w_i}{\sqrt{12}} \approx 0.5 \sqrt{2\,D\,t_D}$$

Combining Equation 1 and Equation 2, the maximum injection plug width w_i^{max} can be calculated by Equation 3, where D is the diffusion coefficient (it is for proteins in the magnitude of approx. 10^{-6} cm^2/s), t_D is the analyte migration time to the detector, ΔP is the applied injection pressure, t_{inj} the injection time, *i.d.* the inner capillary diameter, η the buffer viscosity (approx. 1 mPa s) and L the total capillary length.

Equation 3 Maximum injection plug width w_i^{max}. D = diffusion coefficient of the analyte, t_D = migration time of the analyte to the detector, ΔP = applied pressure, t_{inj} = injection time, *i.d.* = inner capillary diameter, η = viscosity of the BGE, L = total capillary length.

$$w_i^{max} = \sqrt{6\,D\,t_D} = \frac{\Delta P\,t_{inj}\,(i.d.)^2}{32\,\eta\,L}$$

Macromolecules can have diffusion coefficients that are 100 times lower compared to small molecules and need narrower injection plugs [78].

3.2.2 Protein adsorption onto capillary surface and strategies for prevention

One major drawback of CE is the tendency of intact proteins to adsorb onto surfaces, especially the fused silica capillary surface. Adsorption can cause instabilities in the EOF leading to irreproducible migration times. It can also produce band broadening that lowers the separation efficiency, or the recovery of the protein might be reduced by irreversible adsorption making proper quantification unsuccessful [83].

There are several strategies to avoid or at least reduce protein surface binding (*cf.* review [83-85]). One of the simplest ways is to increase the ionic strength of the BGE. The analyte-wall interactions will be reduced as ions in the BGE compete with the analyte for binding sites.

However, high salt concentrations cause joule heating due to an increased current leading to peak broadening and unstable baselines. In addition, high salt amounts are detrimental for MS measurements due to ion suppression and instrument contamination. Consequently, the selection of the sample buffer components is limited to volatile buffer salts [84].

Another approach for reducing adsorption events is the use of surfactants or ion pairing reagents by reducing the protein net charge or making the capillary surface less accessible for the protein. Severe ionization suppression effects can be expected by this method. Therefore, it is not suitable for MS detection [84].

Keeping in mind that adsorption is mainly caused by ionic interactions, the use of BGE with extreme pH values may be a considerable option. At low pH values the silanol groups of the fused silica capillary surface are protonated leading to an almost neutral surface and reducing the possibilities of electrostatic interactions. A weak acidic BGE will lead to deprotonated silanol groups causing electrostatic repulsion for compounds with an overall negative charge, *e.g.* proteins, from the negatively charged surface. In addition, low pH is suitable for ESI-MS detection since the positive ion mode is preferred. However, extreme pH values might lead to conformational changes, degradation or problems with protein solubility [84].

One of the most common approaches to at least reduce protein-surface interactions is to coat the capillary inner wall. These are covalently linked coatings, physically adsorbed polymer coatings and small molecule additives to the BGE. In case of dynamic coatings small molecules or polymers are added to the BGE. They adsorb onto the capillary wall and compete with the analyte proteins for surface binding sites. The coated surface is permanently renewed with subsequently delivery of additives present in the BGE. Therefore, changes in the surface structure that means EOF alterations, are less likely. However, a dynamic coating approach might not be advisable for ESI-MS coupling because of ion source contamination and ion suppression.

Static or semi-permanent adsorbed polymer coatings that need no addition to the BGE seem to be most appropriate for hyphenation to mass spectrometry. Polymer coatings can provide positively charged, negatively charged or neutral surfaces. They can be made of single layers or of altering layers of positive and negative polyelectrolytes.

Several neutral polymers have been described as coating agents for the separation of proteins including poly(ethylene oxide) [86-88], Pluronics block copolymers [89], polyvinylalcohol [87, 90], polyacrylamides [91-95], poly(amine-ester) [96] and cellulose derivates like hydroxypropyl

cellulose (HPC) [97]. The neutral polymer shields the silica surface and reduces the EOF to almost zero.

Cationic coatings are usually prepared by first activating the surface with a NaOH flush to deprotonate the silanol groups and then rinsing the capillary with the polycationic polymer solution. The cationic polyelectrolytes adsorb onto the capillary surface by electrostatic interactions. Positively charged polyelectrolytes induce a reversed EOF. Examples in the literature are polybrene [98, 99], poly(diallyldimethylammonium chloride) (PDADMAC) [100], PolyE-323 [101, 102] or chitosan [103].

In order to produce a negatively charged coating usually a multiple layer strategy is used (successive multiple ionic polymer layer, SMIL). After surface activation and applying a positively charged polymer layer, the capillary is rinsed with an anionic polyelectrolyte. The negatively charged polymer adsorbs onto the positively charged surface due to electrostatic interactions leaving an anionic charge exposed on the surface. The prepared capillary surface induces a normal (cathodic) EOF. The EOF of the prepared surface might be of different magnitude in comparison to the EOF induced by the fused silica surface. The first example of SMIL was with polybrene as first layer followed by dextran sulfate (DS) as terminal layer [98, 104]. Polybrene is the most commonly used polymer for the cationic part of the layer coating, but there are also examples using PDADMAC. The anionic terminal layer consists of poly(vinyl sulfonate) or polystyrene sulfonate beside dextran sulfate [105-107]. The commercially available CEofix [108] coating is commonly used to detect carbohydrate-deficient-transferrin. It is a two-layer SMIL coating. The terminal polyanion coating agent is added to the running buffer and therefore not suitable for MS hyphenation [109, 110].

Although capillary coating can reduce the interaction of the analyte with the surface, complete prevention of adsorption might not be possible for macromolecules such as proteins because functional groups could interact with the surface over electrostatic or hydrophobic interactions [83-85].

3.3 EOF, Capillary coating and Resolution

Equation 4 shows the formula for the resolution R in CE–MS. $\Delta\mu$ is the difference of the migration mobilities of two analytes. Protein isoforms differ only very little in their migration mobilities, resulting in low values of $\Delta\mu$. V is the applied separation voltage. High voltage is necessary for high resolution. The voltage has to be raised by a factor of four to obtain a two-

fold increase in resolution since it is root squared. D is the diffusion coefficient. Proteins have low diffusion coefficients, what is beneficial for the resolution.

Equation 4 Resolution R in CE–MS. $\Delta\mu$ = difference of the migration mobilities of two analytes, V = separation voltage, D = diffusion coefficient of the analyte, $\bar{\mu}$ = mean electrophoretic mobility of two analytes, μ_{EOF} = mobility of the EOF.

$$R = \frac{1}{4\sqrt{2}}\Delta\mu\sqrt{\frac{V}{D\,(\bar{\mu}+\mu_{EOF})}}$$

The analyte resolution not only depends on the differences in electrophoretic mobility of the analytes ($\Delta\mu$), but also on the magnitude of the mean electrophoretic mobility of the analytes in relation to the mobility of the EOF (μ_{EOF}). The resolution of analytes can be improved by selecting an appropriate EOF. $\bar{\mu}$ is the mean mobility of either analyte. When using a charged coating and the analytes are anions there are two scenarios possible. In case of a cationic coating the EOF and the analyte migration are in the same direction, high values are obtained for the term ($\bar{\mu}+\mu_{EOF}$) resulting in low resolution (Figure 7). In case of an anionic coating, the inlet and outlet polarities are switched to get an EOF toward the detector. The analyte is forced in the opposite direction of the EOF. As a result, the term ($\bar{\mu}+\mu_{EOF}$) is low which improves the resolution.
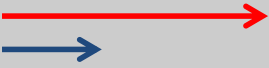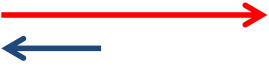
Coating	Inlet polarity	$\bar{\mu}$(analyte mobility) and μ_{EOF}	Outlet polarity	System characteristics
cationic	–		+	robustness: + speed: + resolution: -
anionic (high)	+		–	robustness: + speed: ~ resolution: ~
anionic (low)	+		–	robustness: ~ speed: -- resolution: ++
neutral	–		+	robustness: - speed: - resolution: +

Figure 7 Coating advantages and limitations for the analysis of large anions by CE–MS. Direction and magnitude of the analyte and the EOF are represented by arrows. Adapted from [84].

Very high resolution can be obtained if the magnitude of the EOF and the mobility of the analytes are nearly balancing each other out. Therefore, an anionic coating that induces a low

EOF is necessary. Unfortunately, this comes at the cost of very long analysis times. High resolution can also be obtained with a neutral coating with reduced or zero EOF for slowly migrating analytes, *e.g.* proteins. However, a strong EOF for ESI-MS hyphenation is recommended in order to successfully close the electric circuit and improve ESI spray robustness. In practice, the EOF tuning will be a compromise between resolution, analysis time and stability of the CE–MS hyphenation [84].

3.4 CE and detection with mass spectrometry

In recent years, electrospray ionization has become the predominant ionization method for CE hyphenation to MS. There are two kinds of interfaces used for the coupling either with or without sheath liquid.

The sheath liquid interface is commercially available and most widely used in CE–MS. Here, the separation capillary is encased in a tube of larger diameter in a coaxial setting which provides the conductive sheath liquid (Figure 8). The sheath liquid, to which the CE terminating voltage is applied, mixes with the BGE at the capillary tip. The composition and the flow rate of the sheath liquid are used to support the ionization process. A third coaxial tube provides a sheath gas flow (usually nitrogen gas) to assist the spray formation in the ESI source.
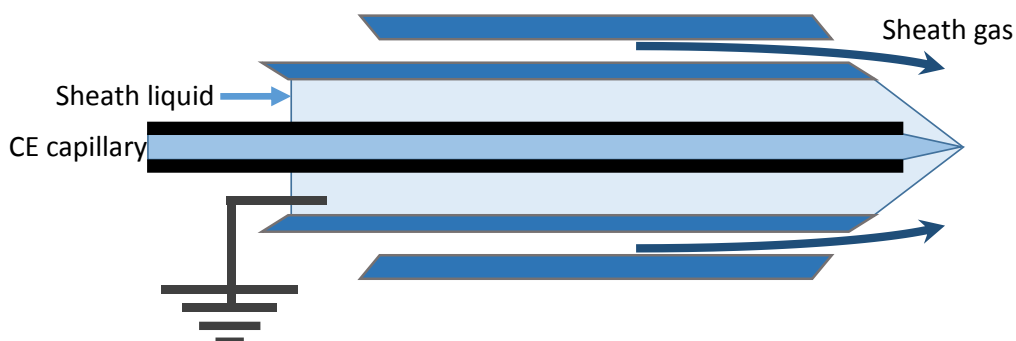
Figure 8 Scheme of the tri-axial CE–MS sheath liquid interface. Adapted from [78].

In the sheathless interface configuration the CE terminating voltage is directly applied to the BGE at the capillary outlet. This can be done by coating the tip of the separation capillary with a metal or by linking the capillary end with a metal-coated, full metal, or conductive sprayer tip. A third way to close the CE circuit is to introduce a microelectrode through the capillary wall into the CE buffer or inserting an electrode at the capillary outlet. Sheathless interfaces are usually linked to nanospray sources leading to more efficient ion formation and higher sensitivity since there is, unlike with sheath liquid interfaces, no dilution effect. However, they tend to be less

robust, flexible and user-friendly than sheath liquid interfaces [84, 111]. A sheathless interface is not commercially available so far.

3.5 Albumin isoform separation by CE

Only a few papers have been published separating isoforms of HSA using CZE. In 1995 Denton and Harris used a commercial neutral coated capillary and 20 mM citrate MES pH 5.2 as a BGE. They obtained 8 peaks with an acceptable resolution. They used ESI-MS as an independent method and *in vitro* degradation procedures in combination with CE to identify four isoforms (intact and *N*-terminally degraded HSA with a free or a blocked Cys34 thiol group respectively). Nevertheless, no data on the reproducibility of their method was provided [112].

In order to reduce the EOF and protein adsorption Girard *et al.* used a phosphate BGE with addition of 1,4-diaminobutane as a dynamic coating. They partly separated variants of HSA and used ESI-MS as an additional method to verify the heterogeneous nature of HSA [113, 114].

Alahmad *et al.* failed in their attempts to reproduce the results from Denton or Girard. Therefore, they developed their own method to separate HSA isoforms. It included a semi-permanent polyethylenglycol coating with a HEPES buffer containing a low concentration of SDS separating 5 peaks and identifying two of them (native and HSA + Cys) by *in vitro* degradation protocols. When adding Cu(II)-ions to the sample mixture, they even obtained nine peaks. The additional peaks indicate a loss of *N*-terminal amino acids, since the amino terminus is known to bind Cu(II) [115].

In the same working group as Alahmad, Marie *et al.* recently published a CE–MS method using a neutral permanent HPC coated capillary and an ammonium bicarbonate separation buffer with or without a low amount of n-dodecyl-β-maltoside. They did not observe any ionization suppression with this BGE. According to them, they separated 9 peaks with low resolution. However, they only showed observed mass data from CE–ESI-MS experiments, no CE–MS electropherogram or mass spectra was shown. Nevertheless, their CE–MS coupling revealed new advanced glycation end products in the HSA preparation. They were able to identify 5 peaks in total (HSA + Cys, native HSA, HSA - L (HSA missing the *C*-terminal leucine), HSA + Cys - L and glycated forms) by CE–UV based on the polyethylenglycol coating in combination with chemical or enzymatic reactions [116].

3.6 Transferrin isoform separation by CE

During the last two decades there has been an interest in separating Tf isoforms by CZE as markers for chronic alcoholism. Individuals with heavy ethanol consumption show elevated ratios of di- and trisialo-Tf in relation to other isoforms in the blood. This condition is called carbohydrate-deficient-transferrin (CDT). The standard method to identify CDT is based on a two layer dynamic coating. An initial capillary rinse with polycationic buffer solution is followed by a rinse with a borate separation buffer containing a polyanion [109, 110]. Dynamic coatings show high stability, but they are not compatible with ESI-MS due to the constant presence of the non-volatile polymers in the BGE. Therefore, detection is usually conducted with UV/Vis at a low wavelength (200 nm) in combination with immunosubstraction methods. UV detection at a low wavelength of 200 nm brings the disadvantage of low selectivity because of interferences of many other biomolecules or solvents. Another drawback of CE–UV is the relatively poor sensitivity due to the short optical pathway given by the inner diameter of the fused silica capillary. Mass spectrometry can improve both shortcomings, the selectivity and sensitivity.

Sanz-Nebot *et al.* used a two-layer coating, Polybrene (5% w/v) and ethylene glycol (2% v/v) as first layer followed by dextran sulfate (3% w/v) as terminal layer together with a BGE of 25 mM ammonium acetate pH 8.5. They partly separated 4 Tf isoforms when injecting an aqueous solution of Tf in the CE–UV mode. The isoform separation deteriorated, when injecting a serum sample, but improved again when the serum was previously treated with an albumin depletion kit. In the CE–MS mode, it was necessary to increase the injected sample volume 3 times. They observed a peak with a partly splitting into 3 isoforms in the total ion current electropherogram. The isoform separation of Tf in the serum sample was worse, even with prior albumin depletion. They assigned some of the found masses in the deconvoluted mass spectra to di-, tetra- and pentasialo-Tf isoforms [117].

In their attempt to develop an ESI-MS compatible method to separate Tf isoforms using CE, Kohler *et al.* recently evaluated numerous coatings and BGEs. With a bilayer coating of 10% polybrene and 10% dextran sulfate in a combination with a basic BGE of 20 mM ammonium acetate at pH 8.5 they were able to partly separate 5 isoforms in the CE–UV mode. When transferring the method to CE–MS no peak was observed with their conventional injection mode. Therefore, they increased the loaded sample volume up to 17 times the volume they injected in the CE–UV mode. However, they observed only one peak. In the deconvoluted mass spectrum they found two masses. They assigned one mass to the most abundant tetrasialo-Tf

(79554 Da) and the other one to disialo-Tf (77214 Da), which has, according to them, a theoretical mass of 77365 Da [118].

4 Experimental

4.1 Materials and methods

4.1.1 Chemicals

Albumin (from human serum - lyophilized powder, essentially globulin free, ≥99% (agarose gel electrophoresis)), apo-Transferrin (human – powder, ≥98% (agarose gel electrophoresis)), poly(diallyldimethylammomium chloride) (PDADMAC) (high molecular weight: weight average molecular weight (M_w) $4 \times 10^5 - 5 \times 10^5$) 20% (w/w) in H_2O, dextran sulfate (DS) sodium salt from *Leuconostoc* spp. (relative molecular weight (M_r) ~ 5×10^5), poly(2-acrylamido-2-methyl-1-propanesulfonic acid) (PAMPS) (M_w 2×10^6) 15% (w/w) in H_2O, hydroxypropyl cellulose (HPC) (M_w~ 10^6, powder, 20 mesh particle size), poly(ethylene glycol)-block-poly(propylene glycol)-block-poly(ethylene glycol) (PEG-PPG-PEG, Pluronic® F-108) (number average molecular weight (M_n) ~ 14600), dichlorodimethylsilane (DSS) (99%), and hydrochloric acid (p.a., 30%) were purchased from Sigma-Aldrich. UltraTrol™ LN dynamic pre-coating solution is commercially available from Target Discovery (Palo Alto, CA, USA). Cisplatin was prepared in house according to a literature procedure [119]. Hexadimethrin bromide (Polybrene) (≥ 94%), sodium hydroxide (~0.1 M, HPCE grade), sodium chloride (puriss. p.a., >99.5%), ammonium hydrogen carbonate (Ultra, >99.5%), sodium dihydrogen phosphate anhydrous (p.a., ≥99.0%), formic acid (puriss. p.a. for mass spectroscopy) and ethylene glycol (puriss. p.a., ≥99.5%) were obtained from Fluka, sodium hydrogen carbonate and ammonium hydroxide (25%, p.a.) from Riedel-de Haën and sodium hydroxide (1 M) from Agilent Technologies. Methanol (HPLC grade), isopropanol and toluene were purchased from Fisher Scientific (Loughborough, UK).

All aqueous solutions were prepared with high purity water (Milli-Q Advantage A10, Merck Millipore, Darmstadt, Germany).

4.1.2 Apparatus

Experiments were performed on a capillary electrophoresis system G7100 (Agilent Technologies, Waldbronn, Germany). UV/Vis detection was carried out with an in-built diode-array detector with a wavelength range from 190–600 nm.

A Julabo F-25 refrigerated/heating circulator was used to adjust the temperature of the CE sample tray.

The pH meter pH 1000 H phenomenal (VWR International, Leuven, Belgium) was used to measure the pH of the buffers.

The direct infusion mass spectra and the CE–ESI-TOF-MS experiments were performed on an ESI-qTOF mass spectrometer (maXis 4G UHR-TOF, Bruker). The coaxial sheath-flow CE ESI-MS Sprayer Kit (G1607A) from Agilent Technologies was used as CE–MS interface.

KDS 100 syringe pump (KD Scientific Inc., Holliston, USA) provided the sheath flow.

The preparation of the HPC coating was done in a GC column oven (6890N Gas Chromatograph, Agilent Technologies) by heating the capillary to 140 °C while flushing it with He gas.

4.1.3 Capillary preparation

Capillaries (fused silica, undeactivated, 50 µm, Agilent Technologies, USA) were cut to a total length of 70 cm, except otherwise stated, with a Shortix™ capillary column cutter (SGT, Singapore) to obtain a clean edge. About 5 mm of the protective polyimide outer capillary coating was taken off at both ends of the capillaries by burning it off with a lighter flame. The UV/Vis detection window was self-made 8.5 cm from the outlet end by burning off about 2 mm of the polyimide layer. In case of CE–MS experiments the UV/Vis detection window was 27 cm from the inlet. The capillary was wiped clean with isopropanol before installation.

4.2 Background Electrolyte

Usually, non-volatile buffers in the BGE such as phosphate buffers give narrower peaks, but when hyphenating to a MS detector they make the electropherograms very noisy, the analyte signal tends to faint and they contaminate the ion source [78]. Therefore, the background electrolyte of choice was ammonium hydrogencarbonate to ensure ESI-MS compatibility. NH_4HCO_3 was dissolved in water in different concentrations. The pH (7.9–8.5) was adjusted with an aqueous solution of NH_3 (25%) to the desired value. The BGE was freshly prepared every day.

4.3 Capillary coatings

All rinse cycles were carried out at approximately 950 mbar. The prepared coating solutions were used within one week and stored at 4 °C.

4.3.1 Cationic coating: Polybrene

Capillary coating was performed by rinsing the capillary (75 µm i.d.) with HCl (1 M for 10 min), water (5 min), NaOH (0.1 M, 10 min), water (5 min), 10 min with an aqueous polybrene solution (10% (w/v), 10 min) and water (5 min). Before the first injection, the capillary was rinsed with BGE for 20 min. Alternatively, a coating solution with Polybrene (10% (w/v)) and ethylene glycol (3% (w/v)) was tested.

4.3.2 Anionic layer coating: Successive multiple ionic polymer layer (SMIL)

Polyelectrolyte solutions were prepared by dissolving the cationic (PDADMAC) or anionic polymers (DS or PAMPS) with a concentration of 0.2% (w/v) in an aqueous solution of 25 mM NH_4HCO_3 1.5 M NaCl at pH 8.5. The coating procedure was performed similar to that described by Nehmé and Perrin [120]. New capillaries were activated by rinsing with HCl (0.1 M), H_2O, NaOH (1 M), NaOH (0.1 M), H_2O for 1 h each. Nehmé and Perrin recommend to carrying out the rinsing cycles with volumes between 50 and 100 times of the capillary volume. The activated capillary was successively rinsed with cationic polyelectrolyte (PDADMAC) solution and anionic polyelectrolyte (DS or PAMPS) solution for 1.5 h each with rinses of H_2O (45 min) in between. After the last (4th) polyelectrolyte rinse the solution was left in the capillary for 1 h. After a final rinse (H_2O 45 min), the capillary was rinsed with BGE for 20 min prior the first run.

4.3.3 Neutral coating

4.3.3.1 UltraTrol^{TM}

In the UltraTrol experiments a capillary with an inner diameter of 75 µm, 58.5 cm total length was used. The coating procedure was similar to the procedure recommended in the user manual [121]. The capillary was activated by rinsing it with HCl (1 M, 5 min), water (2 min), NaOH (1 M, 10 min) and again with water (2 min). The coating was applied by flushing the capillary with UltraTrol solution and the separation buffer for 5 min each.

4.3.3.2 Pluronic

The capillary treatment was modified from Towns and Regnier [122]. New capillaries were flushed with HCl (0.1 M, 15 min), water (5 min), NaOH (0.1 M, 15 min), water (15 min) and methanol (15 min). The capillary was dried in the CE for 3 h at 60 °C while flushing with air. Then it was rinsed with a solution of dichlorodimehtylsilane (DDS, 5% (v/v)) in toluene for 5 min using a syringe. The silylating agent was left in the capillary for 3 h at RT with a 5 min rinse of silylation solution after 1.5 h. In order to flush out the excess of silylating agent the capillary was rinsed with methanol (15 min) and then dried again for 2 h at 60 °C. Afterwards, the capillary was filled with an aqueous pluronic solution (0.5% (w/v)) and statically coated for 2 h. The capillary was flushed with water and BGE for 20 min each prior the first run.

4.3.3.3 Hydroxypropyl cellulose (HPC)

An adapted procedure from Shen and Smith was carried out for the coating with hydroxypropyl cellulose (HPC) [97] with a polymer of higher molecular weight compared to the reference. Longer polymer chains are able to interact with other chains and the capillary surface. Therefore,

they can be expected to induce coatings that are more stable [96]. The capillary was filled with an HPC aqueous solution (0.1% (w/v)) using a syringe. Higher concentrated solutions (*e.g.* 2% (w/v)) did not provide a proper viscosity. The excess solution was flushed out with helium gas at 2 bar pressure while heating the capillary in a gas chromatography oven from 60 °C to 140 °C at 5 °C min^{-1} and holding the temperature at 140 °C for 20 min to obtain a dry polymer layer. The capillary was flushed with water and BGE before use 20 min each. Another coating procedure was tested: The untreated capillary was rinsed with an aqueous solution of 0.1% (w/v) HPC for 5 min. Air pressure was applied and the capillary cassette temperature was raised from 25 to 60 °C in approx. 15 min and kept at 60 °C for 5 h. The capillary was flushed with water and BGE before use 20 min each.

4.4 Sample solutions

Sample solutions, if not otherwise stated, of 600 µM HSA and 30 µM Tf were prepared in a physiological buffer of NaHCO$_3$ (25 mM), NaH$_2$PO$_4$ (4 mM), NaCl (100 mM) at pH 7.4. To avoid possible denaturation only moderate motion was used to dissolve the proteins in the sample buffer. For interaction experiments, sample solutions with cisplatin were prepared in the physiological sample buffer, and sonicated to dissolve the platinum complex. The cisplatin solution was mixed with a freshly prepared protein mixture to obtain final concentrations of 600 µM for HSA and cisplatin and 30 µM for Tf. The injection of the first run, in case of sequential runs, was within five minutes after preparation.

4.5 Operating conditions

4.5.1 CE–UV/Vis

CE experiments with UV/Vis detection were carried out to determine suitable capillary coating conditions for MS hyphenation. The samples were hydrodynamically injected for 5 s at 20 mbar leading to an injection volume of approximately 2.2 nL (for a 50 µm i.d., 70 cm capillary) for all CE–UV/Vis experiments. The injection conditions were determined by using the formula for the maximum injection width that does not significantly contribute to zone broadening (Equation 3). The separation was tested by performing runs at numerous different potentials. In the case of negative charged capillary surfaces +20 kV turned out to be best suited, -30 kV gave best results for neutral coatings. The temperature of the sample tray was adjusted to 37 °C or to room temperature in case of method development and the capillary temperature was set to 25 °C. All shown CE–UV electropherograms are recorded at 200 nm. Electrochemical processes can alter the pH of the running buffer leading to migration time changes when a voltage is applied.

Therefore, the BGE solution in the separation vials was replenished before every run. Before every run, the capillary was rinsed with BGE (2 min) to fill the capillary with fresh separation buffer and after every run with water (4 min) and BGE (1.5 min) to detach potentially adsorbed proteins.

4.5.2 ESI-qTOF-MS

High resolution mass spectrometry was performed on a Maxis UHR ESI-qTOF instrument (Bruker Daltonics GmbH, Bremen, Germany). Tf was dissolved in water at a concentration of 100 µM for MS direct infusion. The aqueous Tf solution was diluted with MeOH/H_2O (50:50 (v/v), 2% formic acid) 10 times and injected by direct infusion into the mass spectrometer using a KDS 100 syringe pump at a flow rate of 3 µL/min. Dry temperature was set to 220 °C and dry gas flow rate was 6.0 L/min. Nebulizing gas was set to 6 psi. The applied ESI voltage was set to –4 kV. MS detection was executed between 1000 and 4000 *m/z*, and 2 spectra/s were acquired. Mass spectra were recorded over 0.4–0.8 min and averaged. MS data was analyzed using DataAnalysis 4.0 software from Bruker Daltonics GmbH. Mass spectra were deconvoluted with the maximum entropy deconvolution algorithm using automatic data point spacing, 30 000 resolving power and no smoothing.

4.5.3 CE–ESI-qTOF-MS

PDADMAC/PAMPS, PDADMAC/DS and Pluronic coated capillaries were used for CE–MS experiments. BGE was either 25 mM NH_4HCO_3 pH 8.5 or 100 mM NH_4CO_3 pH 7.9. Hydrodynamic injection of 20 mbar for 5 s that was used in the CE-UV/Vis was raised to 50 mbar for 30 s (approx. 33 nL) because of sensitivity issues. CE was coupled to MS *via* a coaxial sheath-flow ESI interface from Agilent Technologies. The sheath liquid was composed of methanol-water (50:50 (v/v), 2% formic acid) and was delivered *via* a KDS 100 syringe pump at a flow rate of 3 µL/min. Other MS conditions were identical compared to section 4.5.2.

5 Results and discussion

In order to imitate biological conditions a sample mixture of albumin and transferrin was prepared in one vial in a buffer with comparable composition, concentrations and pH to the human serum. Accordingly, the concentrations of HSA and Tf were 600 μM and 30 μM, respectively, at a pH of 7.4. The buffer contained 4 mM phosphates, 25 mM carbonates and 100 mM sodium chloride. The most abundant Tf isoform, tetrasialo-Tf, has a pI of 5.4 and every additional sialic acid group lowers the pI by approx. 0.1, every sialic acid less raises the pI by approx. 0.1 [61]. The recently reported pI (by Turrel) for albumin is approx. 4.9 for native HSA, approx. 4.8 for oxidized HSA and a pI in between for HSA with mixed disulfides [10]. The pH of the BGE (7.9 or 8.5) above the pI of the proteins was chosen to ensure a negatively charged state for all protein species in the injected sample. As the size of the albumin isoforms and transferrin isoforms is similar, it is more likely to separate them in an electric field, when they differ in their total charge.

As already mentioned, the separation in CE is based on the *charge-to-size* ratio of the analytes. In case of Tf, when a carbohydrate branch with a sialic acid group is added to a Tf isoform the total mass and size of the large protein only changes very little. This means that the electrophoretic mobilities based on the *charge-to-size* ratio of these two isoforms will also differ little even when there is a negative charge added with an additional sialic acid group. In order to make a separation possible it is necessary to lower the EOF by adjusting the capillary surface charge as described in section 3.3.

First, different capillary coatings were tested in the CE–UV/Vis mode. During method development, single runs were repeated at least once. The coatings with the most promising results in case of separation performance where further investigated with respect to their stability. Coating stability was tested by executing sequential runs with the same protein sample over 24 h and included 33 runs with anionic coatings and 29 runs in case of neutral coatings. These experiments were repeated on a newly coated capillary. The EOF and analyte mobilities were compared with respect to their RSD. Instead of an EOF marker, which is usually an uncharged molecule such as dimethylsulfoxide, a system peak was chosen for EOF monitoring to exclude a possible interaction with the capillary coating or the analyzed proteins. The coatings showing the most promising results with respect to protein isoform separation and coating stability were chosen for interaction experiments with cisplatin over 24 h. Further experiments were conducted with CE hyphenated to ESI-MS. The tested samples for coating stability, interaction with cisplatin and CE–MS were incubated in the sample tray at 37 °C.

5.1 Method development by CE–UV

Several capillary surface conditions were investigated for the separation of albumin and transferrin isoforms within one electrophoretic run, which are described in this chapter.

5.1.1 Bare fused silica

The starting point was a bare fused silica capillary. When using an alkaline BGE the silanol surface is negatively charged. A mixture containing transferrin and albumin was separated into two peaks, but without isoform separation (Figure 9) (average $\mu_{EOF}=6.35 \cdot 10^{-4}$ cm^2 V^{-1} s^{-1}, RSD 1.17%, average $\mu_{Tf}=5.35 \cdot 10^{-4}$ cm^2 V^{-1} s^{-1}, RSD 1.20%, average $\mu_{HSA}=4.44 \cdot 10^{-4}$ cm^2 V^{-1} s^{-1}, RSD 1.30%, n=2).
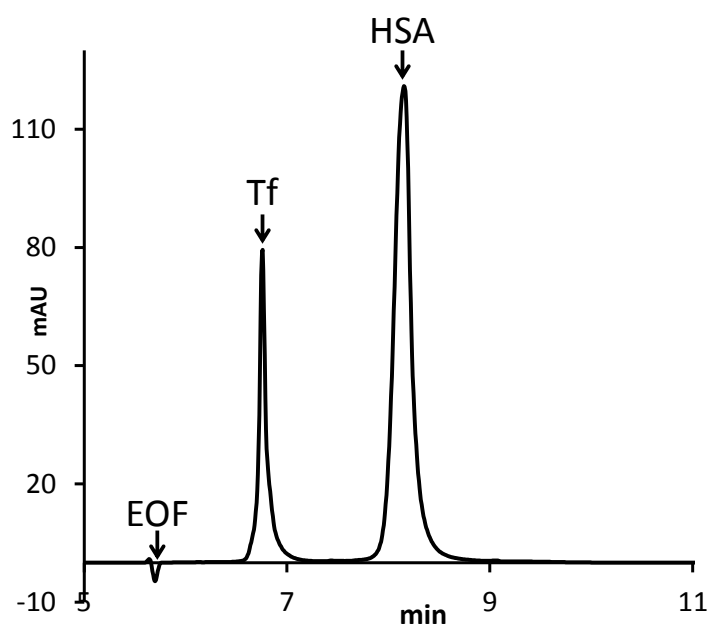
Figure 9 UV-Electropherogram of HSA/Tf mixture with an uncoated bare fused silica capillary (70 cm total length, 50 µm i.d.). BGE: 25 mM NH₄HCO₃ pH 8.5, 20 kV.

5.1.2 Cationic coating: Polybrene

A cationic polybrene (hexadimethrine bromide, Figure 10) coating with an alkaline BGE increased the protein/surface interactions indicated by severe peak tailing and baseline shift (Figure 11). A BGE with an acidic pH would have decreased the protein/surface attraction. However, in that case the different albumin or transferrin isoforms would not differ in their total charge and separation would be impossible. A polybrene coated capillary with an addition of ethylene glycol in the coating solution gave similar results (data not shown). Therefore, positively charged surface coatings were not further investigated.

Hexadimethrine bromide (Polybrene)
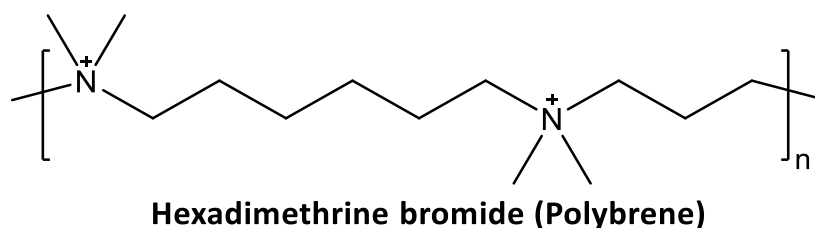
Figure 10 Structure of the positively charged polymer hexadimethine bromide (polybrene).
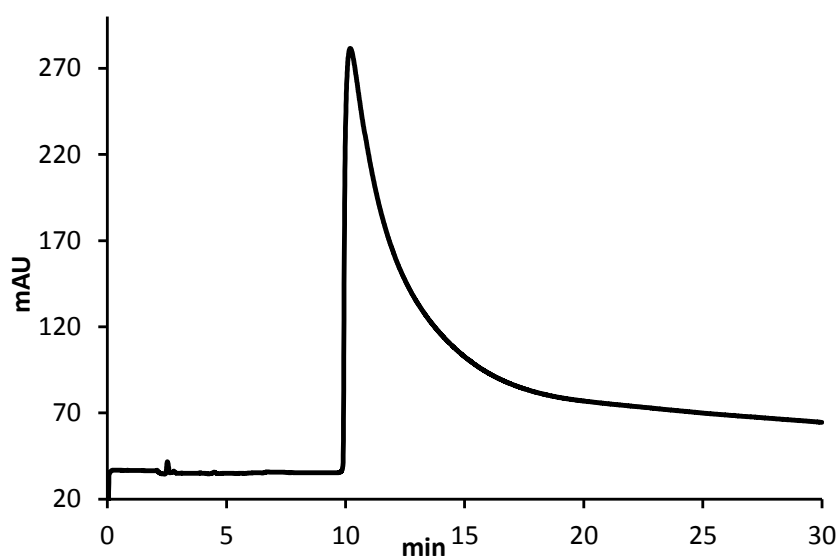
Figure 11 UV-Electropherogram of HSA/Tf mixture with a polybrene coated capillary (70 cm total length, 75 μm i.d.). BGE: 25 mM NH_4HCO_3 pH 8.5, -30 kV.

5.1.3 Anionic coatings

The inner surface of the capillary was activated by flushing with NaOH. In order to generate the anionic layer coatings the activated capillary was first rinsed with a cationic polymer solution, then with an anionic polymer solution. The cationic layer consists of PDADMAC (Figure 12). The anionic layer was either Dextran sulfate or PAMPS (Figure 13). This procedure results in a two-layer coating with a negatively charged surface. When repeating these steps a 4-layer coating can be generated. The 4-layer coating showed higher stability indicated by lower EOF and migration time shifts. Both terminal anionc coatings with 4 layers were investigated with respect to their stability over 24 h.

**Poly(diallyldimethyl-
ammonium chloride)
(PDADMAC)**
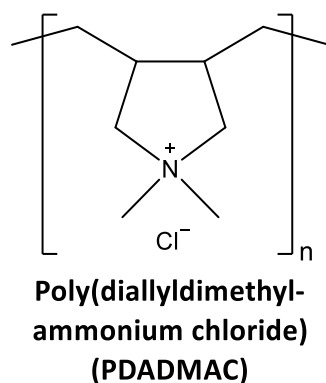
Figure 12 Structure of the positively charged polymer poly(diallyldimethylammonium chloride) (PDADMAC).

R = SO_3Na or H
**Dextran sulfate
(DS)**

**Poly(2-acrylamido-2-methyl-
1-propanesulfonic acid)
(PAMPS)**
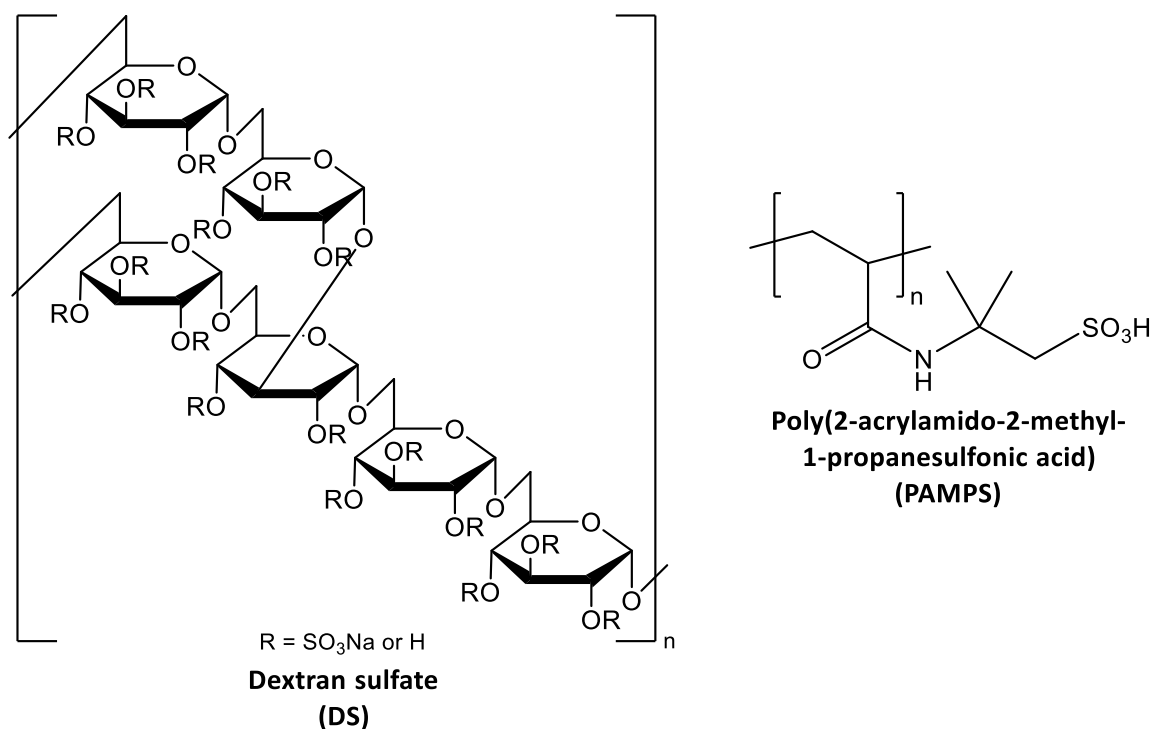
Figure 13 Structures of the negatively charged polymers.

5.1.3.1 Dextran sulfate (DS)

The isoforms of Tf and HSA start to separate when a 4-layer coating of PDADMAC as intermediate layer and Dextran sulfate as the terminal coating layer was applied. However, the migration times increase with the number of runs which is more pronounced for later migrating analytes (Figure 14) (average μ_{EOF}=3.94·10^{-4} cm^2 V^1 s^{-1}, RSD 1.39%, average μ_{Tf}=2.88·10^{-4} cm^2 V^{-1} s^{-1}, RSD 2.21%, average μ_{HSA}=1.89·10^{-4} cm^2 V^{-1} s^{-1}, RSD 3.82%, n=33). The Tf

peak shows a beginning separation of the most abundant tetrasialo-Tf isoform from the lower abundant isoforms indicated by the broad bottom of the peak. The HSA peak partly separates into two peaks, which is best visible in the orange track after 24 h. There is also a smaller broad peak with a higher migration time.
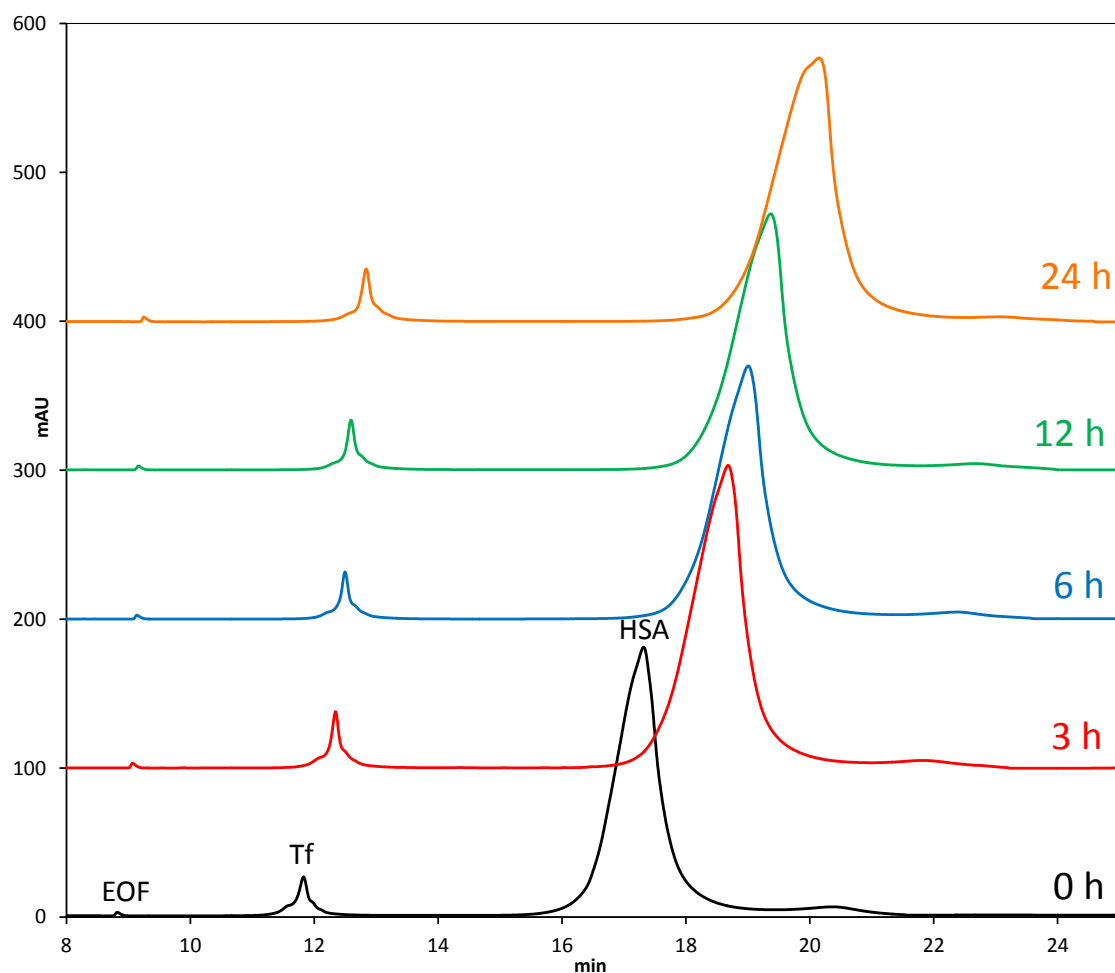
Figure 14 UV-Electropherograms, serial runs over 24 h of HSA/Tf mixture with a layer coated capillary with DS as terminal layer (70 cm total length, 50 μm i.d.). Sample tray temperature 37 °C, BGE: 25 mM NH₄HCO₃ pH 8.5, 20 kV.

In the literature, the procedure of CE method development of transferrin or albumin isoform separation experiments includes commercially available lyophilized protein that is dissolved in water without any addition of salt, containing all isoforms [116-118]. Therefore, a sample without NaCl in the sample buffer was additionally tested (Figure 15) for comparison to literature data, where DS is commonly used as a last layer coating agent [117, 118] (average μ_{EOF}=3.94·10^{-4} cm^2 V^{-1} s^{-1}, RSD 1.90%, average μ_{Tf}=2.88·10^{-4} cm^2 V^{-1} s^{-1}, RSD 3.62%, average μ_{HSA}=1.87·10^{-4} cm^2 V^{-1} s^{-1}, RSD 7.71%, n=33). The isoform separation of HSA is slightly less

effective as the major peak is more symmetrical in the earlier runs. In the later runs (see exemplary 12 h and 24 h run in Figure 15) it is already visible, that the peak consists of at least two isoforms. A smaller broad peak with a later migration time also occurs. Peak tailing and an increased baseline after the peak indicate protein capillary surface interactions, but secondary peaks may also occur because of delayed desorption of adsorbed proteins [123, 124]. Therefore, the small broad peak with highest migration time on the DS coating might also be a sign for protein adsorption on the DS coating.
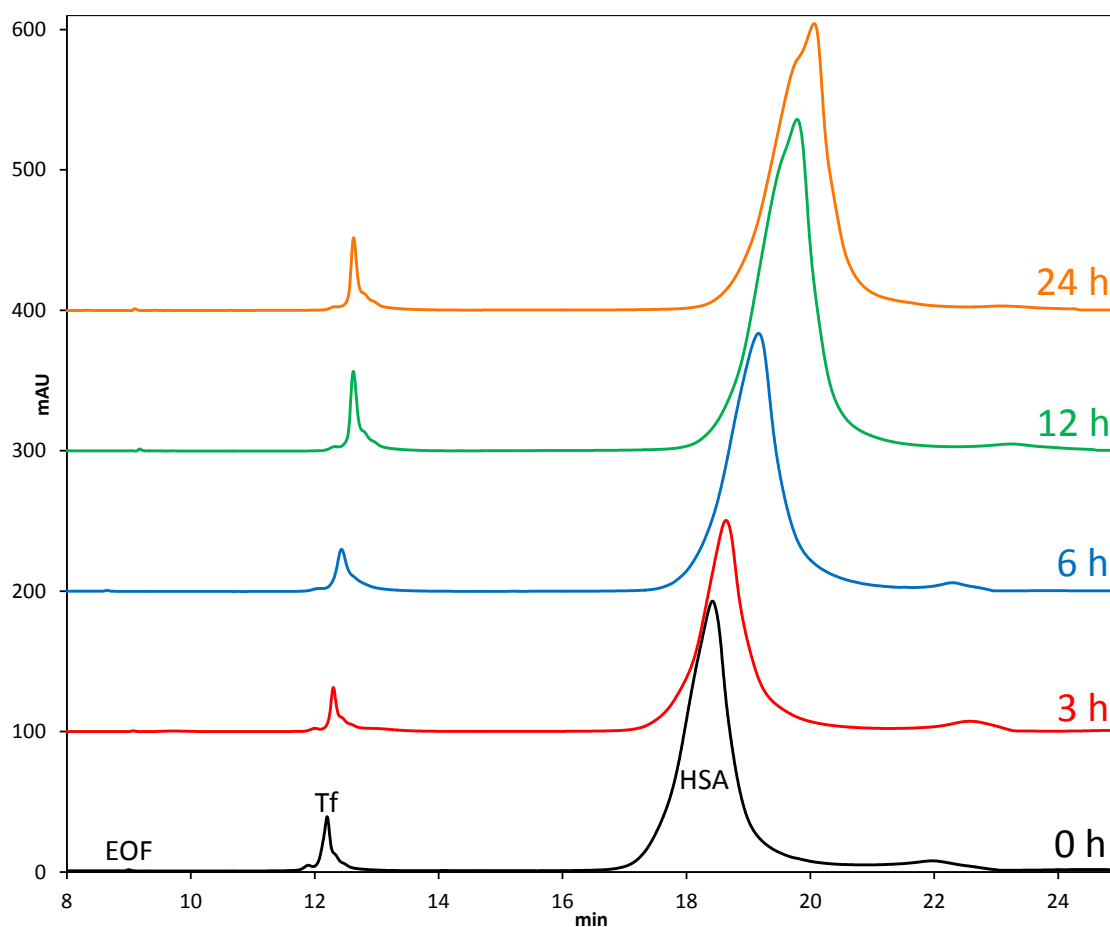
Figure 15 UV-Electropherograms, serial runs over 24 h of HSA/Tf mixture without NaCl with a layer coated capillary with DS as terminal layer (70 cm total length, 50 µm i.d.). Sample tray temperature 37 °C, BGE: 25 mM NH_4HCO_3 pH 8.5, 20 kV.

Figure 16 shows a comparison of the section of the Tf peak of two electropherograms; (A) is from the HSA/Tf in the sample buffer with NaCl, (B) is from the HSA/Tf in the sample buffer without NaCl. The lower charged Tf isoforms, most likely di- and trisialo-Tf (2/3), have an improved separation from the tetra- and higher-sialo-Tf isoforms when there is no addition of NaCl in the sample buffer. However, for realistic interaction experiments with cisplatin, it is

essential to have conditions that are similar to the conditions in the blood stream. The chloride concentration is important to ensure a comparable hydrolysis rate of cisplatin to that in the bloodstream [125, 126]. Therefore, a sample buffer with chloride and a pH of 7.4 was chosen to dissolve the proteins for all experiments.
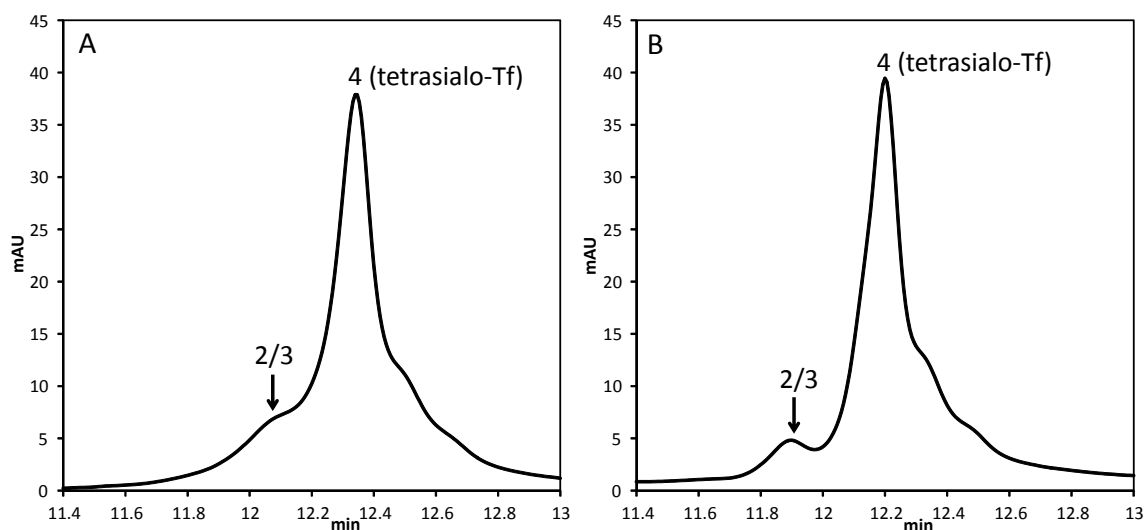
Figure 16 Enlarged Tf peak section of UV-electropherograms with a layer coated capillary with DS as terminal layer (70 cm total length, 50 µm i.d., BGE: 25 mM NH_4HCO_3 pH 8.5, 20 kV) of HSA/Tf mixture in (A) the regular sample buffer with 100 mM NaCl and (B) without NaCl in the sample buffer.

5.1.3.2 Poly(2-acrylamido-2-methyl-1-propanesulfonic acid) - PAMPS

With PAMPS providing the anionic surface of the 4-layer coating the migration times show good consistency over 24 h (average μ_{EOF}=4.31·10^{-4} cm^2 V^{-1} s^{-1}, RSD 0.50%, average μ_{Tf}=3.24·10^{-4} cm^2 V^{-1} s^{-1}, RSD 0.36%, average μ_{HSA}=2.27·10^{-4} cm^2 V^{-1} s^{-1}, RSD 0.36%, n=33, Figure 17). The broad bottom at the transferrin peak indicates the starting separation of lower abundant isoforms from the major tetrasialo-Tf isoform. The albumin peak shows again a beginning separation into two peaks.
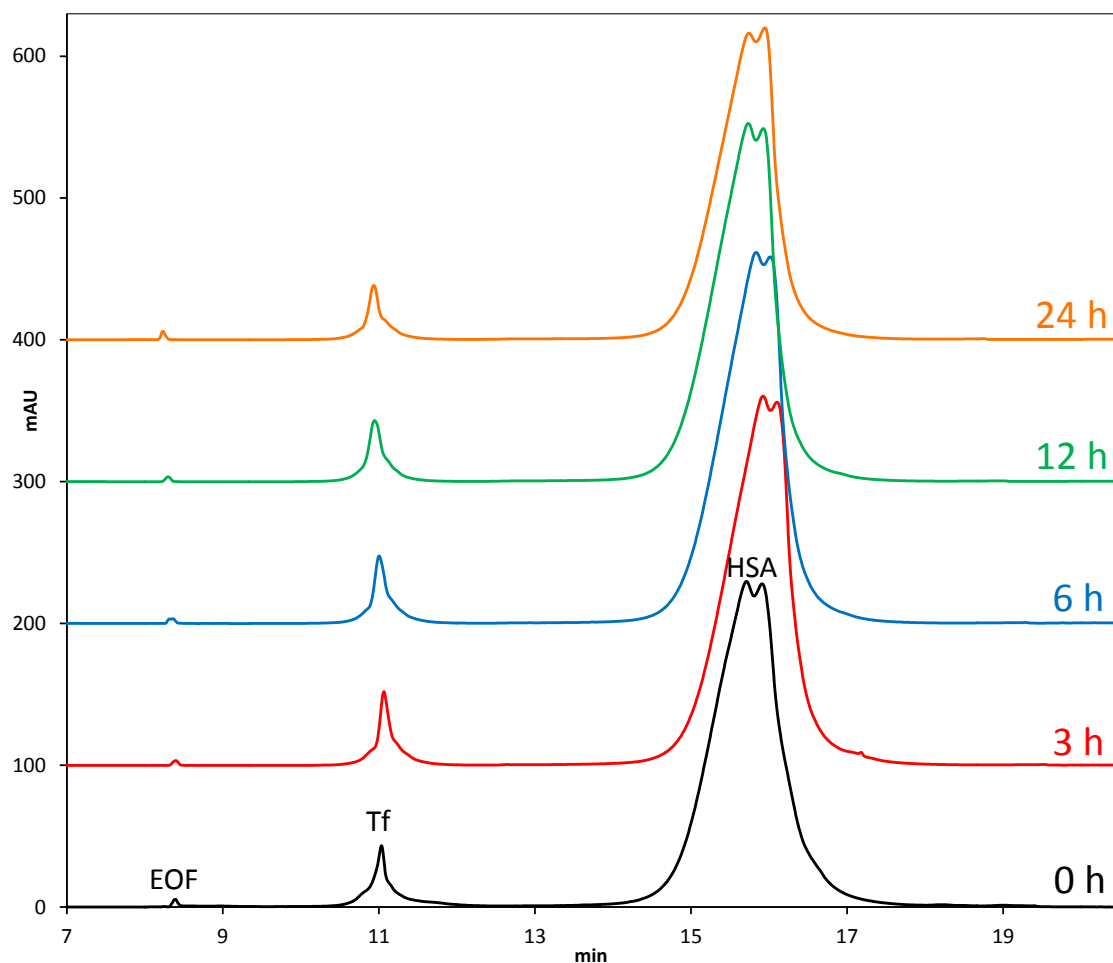
Figure 17 UV-Electropherograms, serial runs over 24 h of HSA/Tf mixture with a layer coated capillary with PAMPS as terminal layer (70 cm total length, 50 µm i.d.). Sample tray temperature 37 °C, BGE: 25 mM NH$_4$HCO$_3$ pH 8.5, 20 kV.

5.1.4 Neutral coatings

The negatively charged terminal coatings generate an EOF with a higher magnitude than the effective electrophoretic mobilities of the analyte anions. When positive voltage is applied the EOF forces the whole bulk solution toward the detector. On the other hand, neutral coatings are inducing an EOF that is almost zero. Consequently, the total migration of the analytes is made up mostly by the effective mobility of the proteins alone and a negative voltage is mandatory for anions to reach the detector. This results in an improved resolution, in case the analyte mobilities are significantly different from each other. The migration order is reversed and HSA is reaching the detector before Tf.

5.1.4.1 UltraTrol^TM LN

The commercially available dynamic pre-coating UltraTrol^TM LN delivered the so far best separation performance with respect to Tf. Although not base-line separated, the low-abundant isoforms of Tf are clearly visible and span from the disialo- to the octasialo-Tf (Figure 18). Most abundant was again tetrasialo-Tf, together with the penta- and hexasialo forms. The migration order was reversed in comparison to anionic coated capillaries. The peak assignment was made by comparison of migration order and relative abundance of Tf isoforms with literature data [127]. Unfortunately, the coating is not stable. As described in the UltraTrol^TM user manual [121], the capillary has to be rinsed between runs with 1 M NaOH, to strip off the coating and the adsorbed protein. After a rinse with water the capillary has to be recoated, by rinsing again with coating solution, and with separation buffer before the following sample injection. The recoating step would not be suitable for CE–ESI-MS hyphenation disqualifying this coating for further investigation. HSA isoform separation was not investigated on an UltraTrol coated capillary.
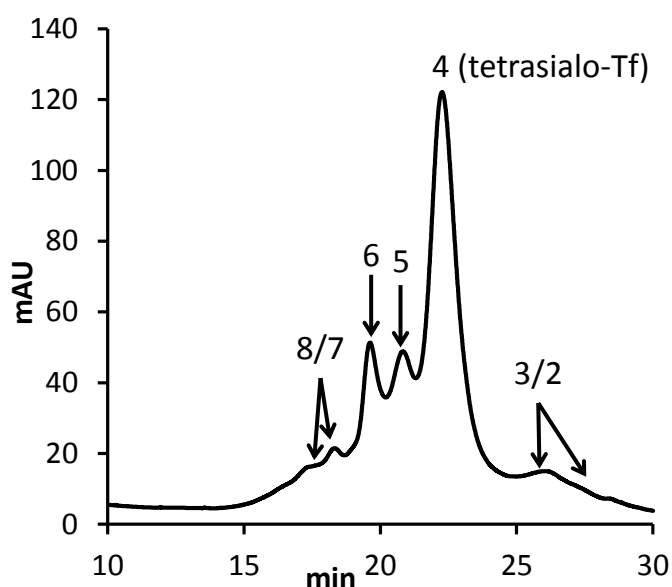
Figure 18 Electropherogram of 30 µM transferrin in 20 mM NaHCO$_3$ with an UltraTrol coated capillary (58.5 cm total length, 75 µm i.d.). Injection: 30 mbar 5 s, BGE: 30 mM NH$_4$HCO$_3$ pH 8.5, -25 kV.

5.1.4.2 Poly(ethylene glycol)-block-poly(propylene glycol)-block-poly(ethylene glycol) - Pluronic

The cleaned and dried capillary surface was first treated with a solution of dichlorodimethylsilane (DDS) in toluene before coating it with the Pluronic block polymer (Figure 19). DDS is able to react with the silanol groups of the silica surface and increase its hydrophobicity. Due to hydrophobic interactions the poly(propylene glycol) part of the Pluronic

copolymer adsorbs onto hydrophobic surfaces, while the hydrophilic poly(ethylene glycol) chains extend into the aqueous bulk solution [89, 128, 129].
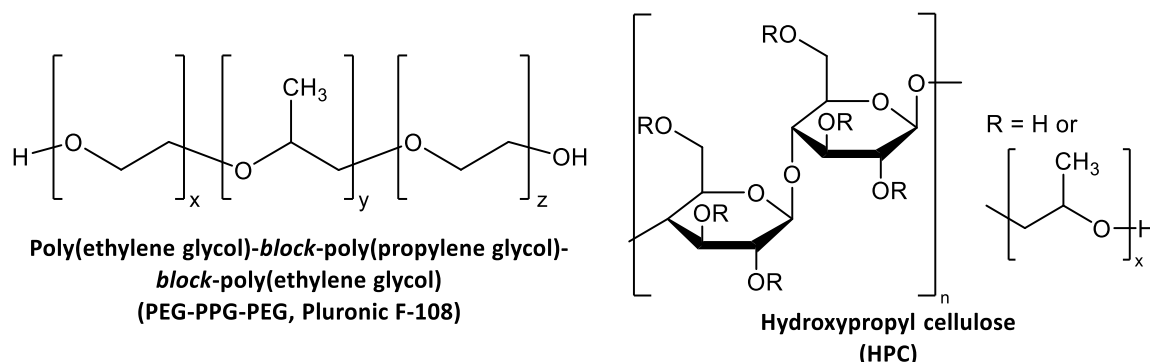
Figure 19 The neutral polymers used during method development are Pluronic F-108 (*left*) and HPC (*right*).

Preliminary experiments showed a beginning isoform separation of the HSA/Tf mixture. The effect of ionic strength and the pH of an ammonium bicarbonate BGE were investigated with respect to isoform separation (Figure 20).

A beginning separation of HSA into two peaks (Figure 20B black track) is already visible with the standard BGE (25 mM NH_4HCO_3 pH 8.5). The shoulders of the Tf peak already indicate various isoforms (Figure 20C black track). A lower pH of 7.9, but identical concentration, results in better separation as indicated by the HSA peak in the red track. When increasing the ionic strength to 100 mM NH_4HCO_3, transferrin (lower mobility, Figure 20C purple track) separates into one major peak most likely containing tetrasialo-Tf, and at least 4 smaller peaks (see also Figure 22A). In the case of albumin there is a starting separation into a major peak, the native HSA, and a smaller peak with an earlier migration time, probably glycated forms (Figure 20B purple track). The shoulder at a higher migration time should be mostly composed of HSA with a cysteinylated Cys34. The peaks were assigned on basis of the migration order and relative abundance of isoforms reported in the literature (see also Figure 22) [116, 127]. It is of note that higher buffer concentrations lead to improved separation of the HSA and Tf isoforms.

42
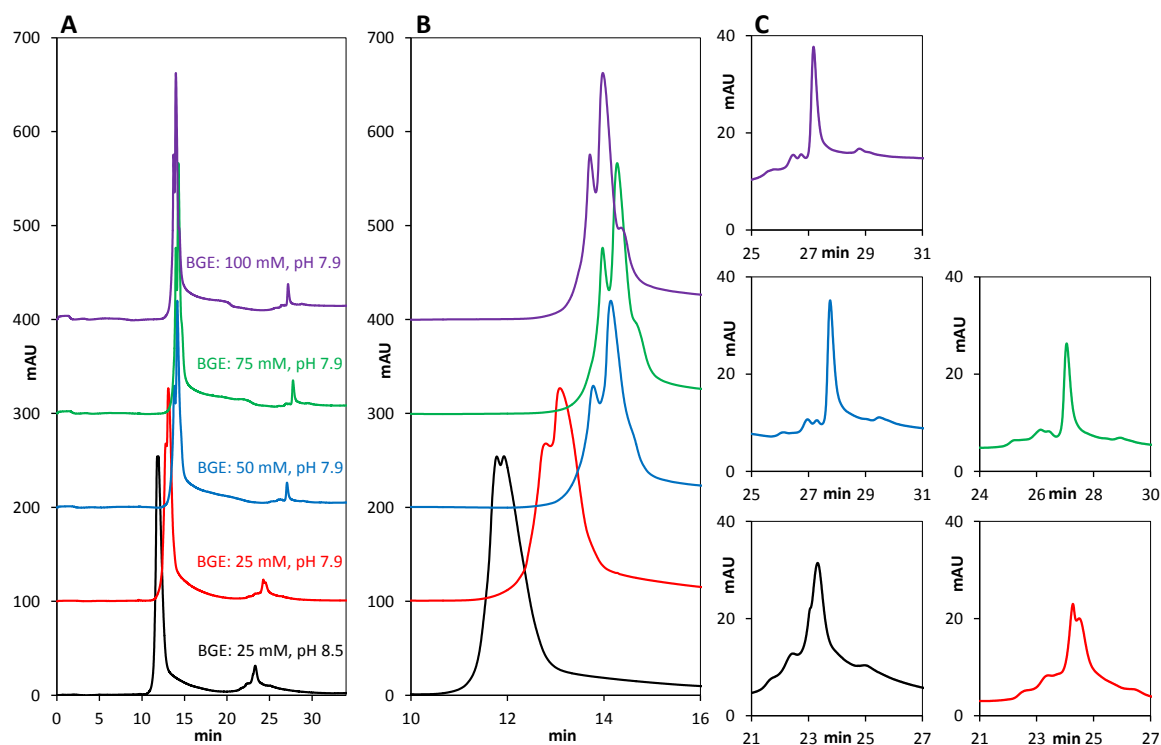
Figure 20 UV-Electropherograms of BGE optimization on a pluronic coated capillary (70 cm total length, 50 μm i.d). (A) Different ionic strengths and pHs of the NH_4HCO_3 BGE, separation voltage -30 kV. (B) Enlarged section of HSA peaks. (C) Enlarged section of Tf peaks.

The performance of the pluronic coating was tested over 24 h with the BGE containing 100 mM NH_4HCO_3 at pH 7.9 because it showed the best separation. A total of 29 sequential injections and separation runs were carried out (average μ_{Tf}=-0.82·10^{-4} cm^2 V^{-1} s^{-1}, RSD 1.33%, average μ_{HSA}=-1.69·10^{-4} cm^2 V^{-1} s^{-1}, RSD 1.06%, n=29).
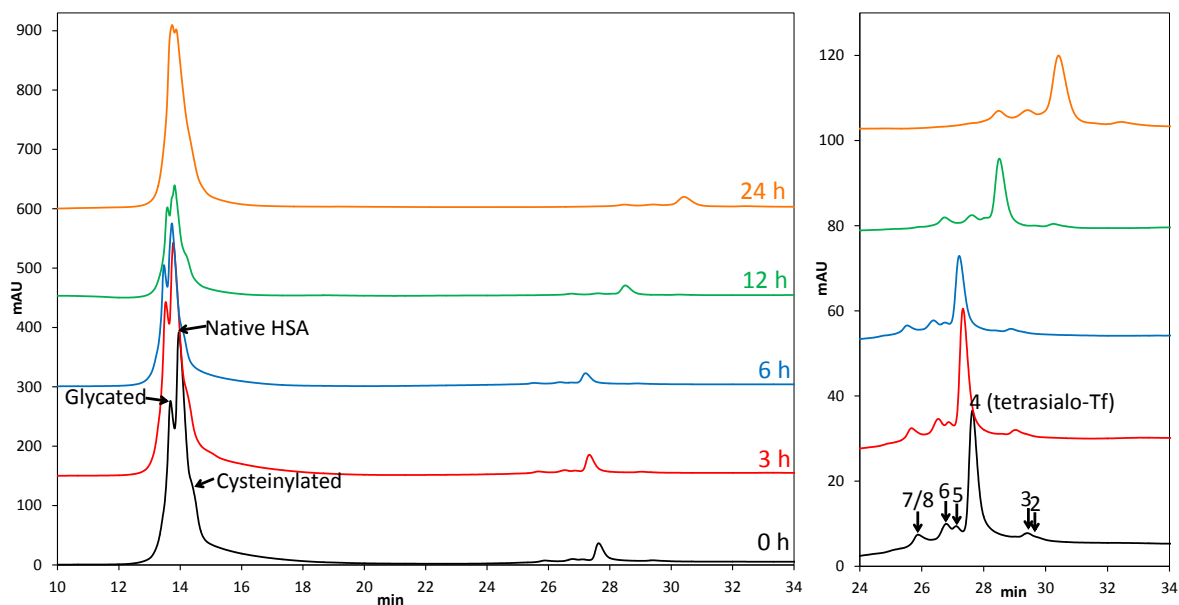
Figure 21 UV-Electropherograms of sequential runs over 24 h of a HSA/Tf mixture with a pluronic coated capillary (70 cm total length, 50 μm i.d.). Enlarged section of Tf peaks on the right hand side. Sample tray temperature 37 °C, BGE: 100 mM NH_4HCO_3 pH 7.9, -30 kV.

5.1.4.3 Hydroxypropyl cellulose (HPC)

The neutral coating with hydroxypropyl cellulose (HPC) (Figure 19) was mounted onto the capillary by heating it in a gas chromatography oven at 140 °C and flushing it with helium. The hydroxyl groups on the substituted hydroxyalkyl chains are able to react with the remaining hydroxyl groups on the substituted chain to obtain stable ether bonds. In addition to the intra- and interchain reactions, chemical reactions between the HPC residues and the fused silica capillary wall can also occur [97]. These linkages are supposed to be responsible for higher coating stability [96]. The separation results were very similar for a coating procedure including a drying step in an airstream at 60 °C for 5 h (data not shown).
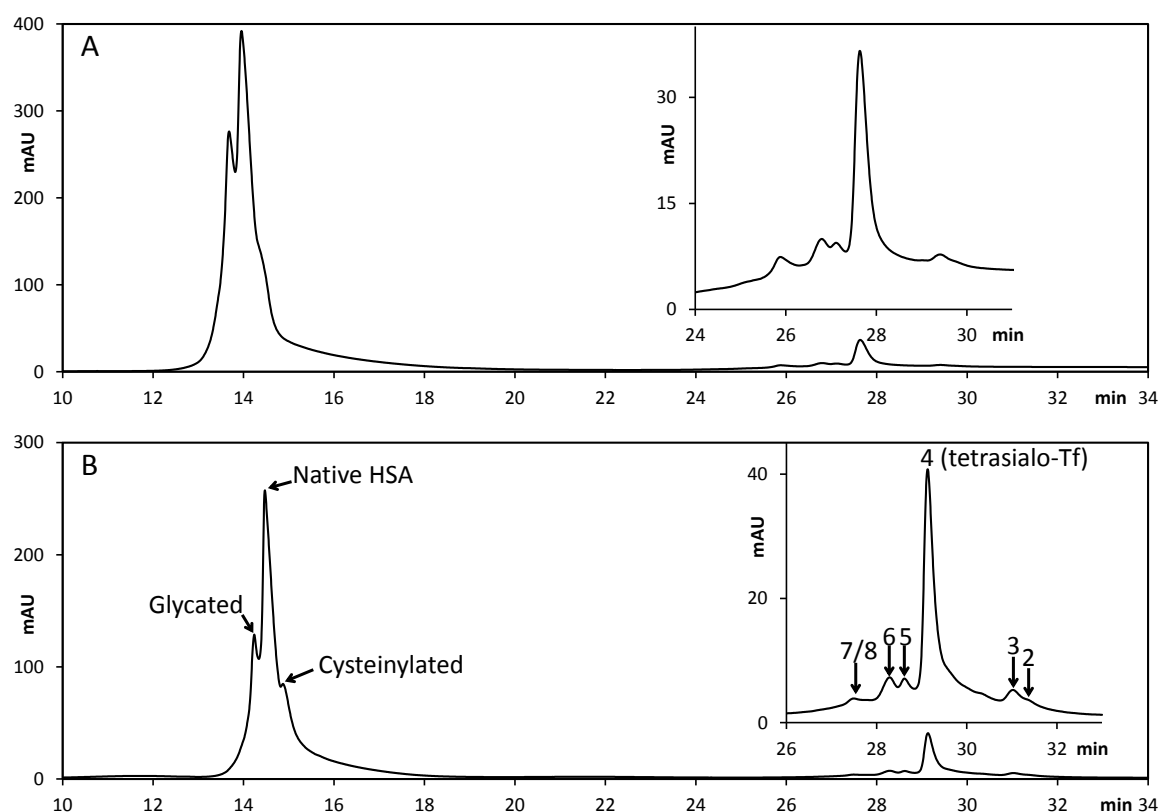
Figure 22 Electropherograms of HSA/Tf mixtures with different neutral coated capillaries (70 cm total length, 50 μm i.d.). BGE: 100 mM NH$_4$HCO$_3$ pH 7.9, -30 kV. (A) Pluronic coated capillary. (B) HPC coated capillary. The insets show the isoforms of Tf.

Figure 22B shows the electropherogram of a HSA/Tf mixture with a HPC coated capillary. The resolution of HSA isoforms was improved in comparison to the pluronic coating (Figure 22A), while the separation of the Tf isoforms did not further improve. Interestingly, the mobilities of both proteins are slightly lower in case of the HPC coating. This might indicate a slightly lower EOF for the HPC coating compared to the pluronic coating. The HPC might not completely shield the charge of the fused silica capillary to suppress the EOF of the HPC. While the resolution for the HPC coating was better than for the pluronic coating, it was not as stable (Figure 23) (average μ$_{Tf}$=-0.74·10^{-4} cm^2 V^{-1} s^{-1}, RSD 8.69%, average μ$_{HSA}$=-1.59·10^{-4} cm^2 V^{-1} s^{-1}, RSD 3.47%, n=13). The quality of the HSA and Tf peaks deteriorates over time and the migration times are also shifting dramatically. Sequential runs were aborted after 13 runs (10 h), because of the substantial increase in runtime. Hence, the HPC coating was not investigated with respect to MS coupling.
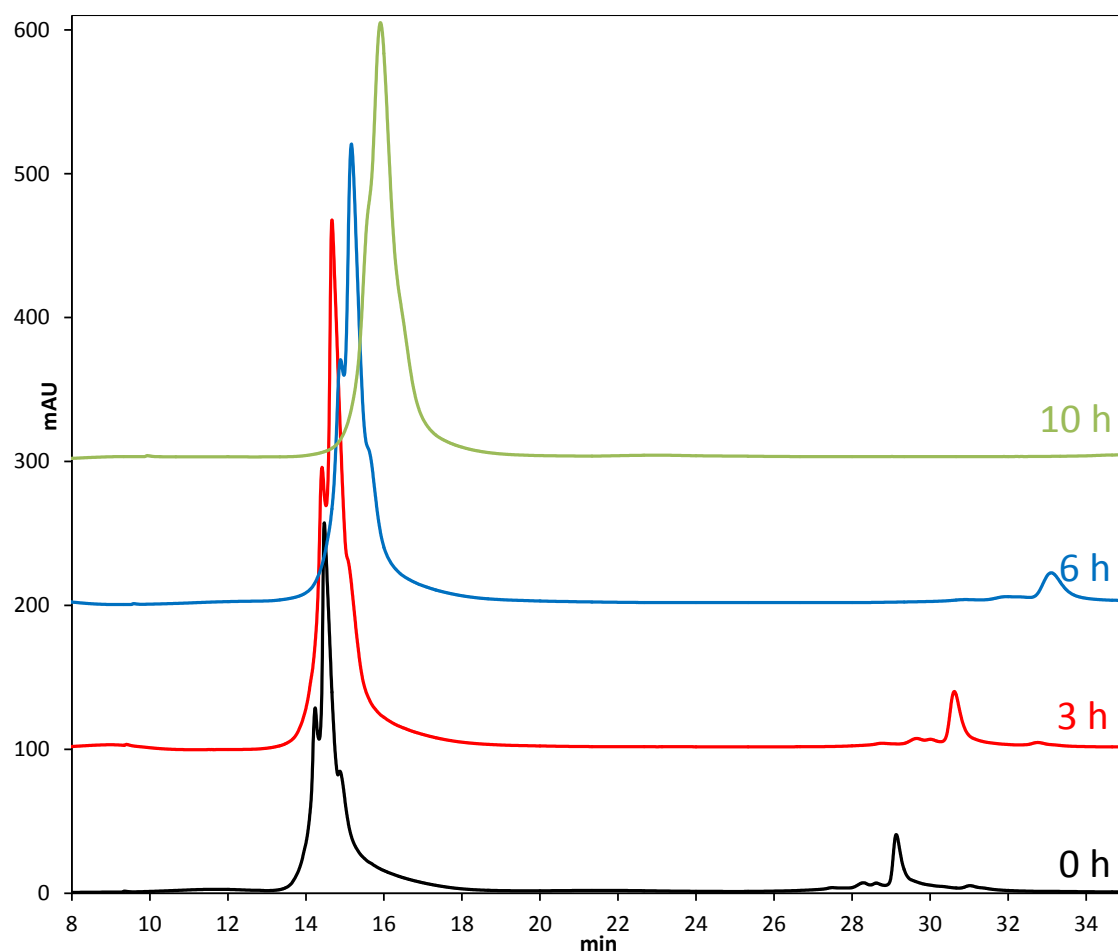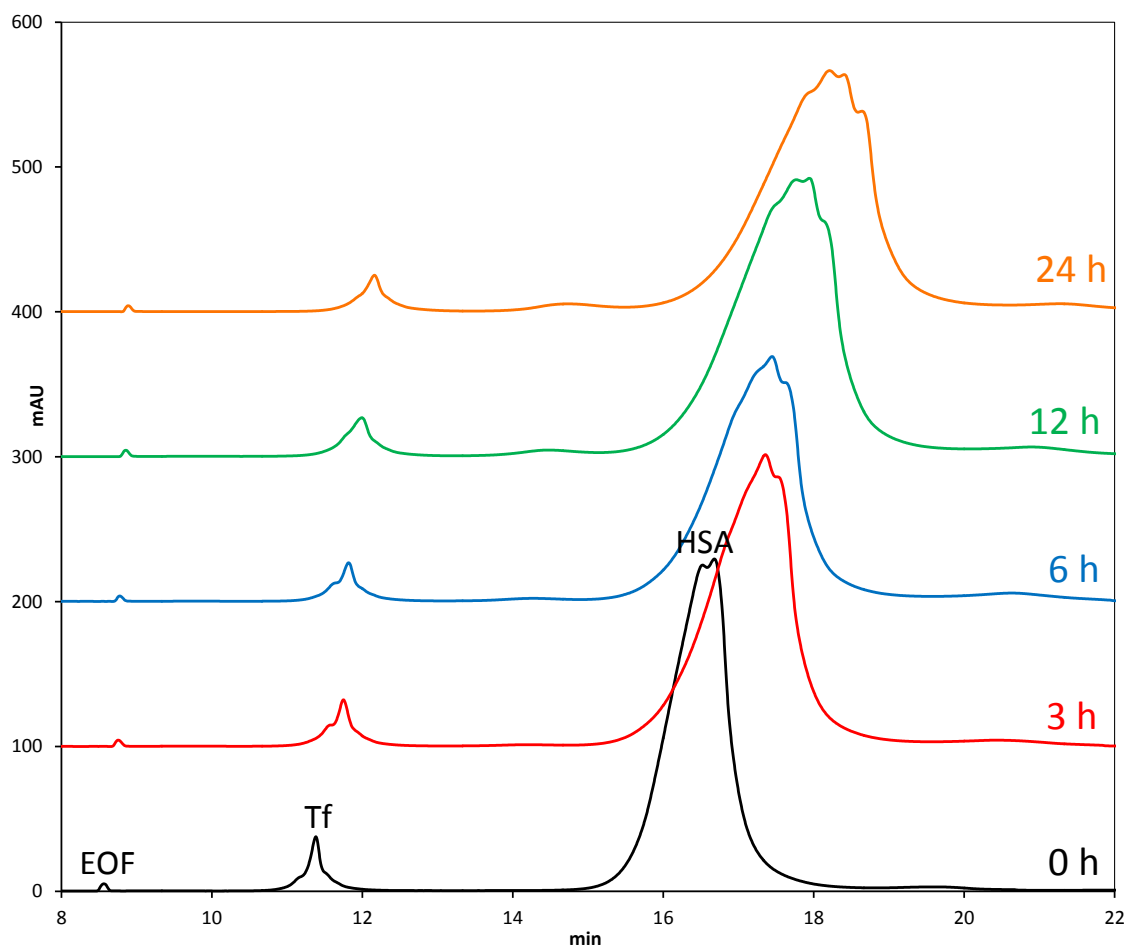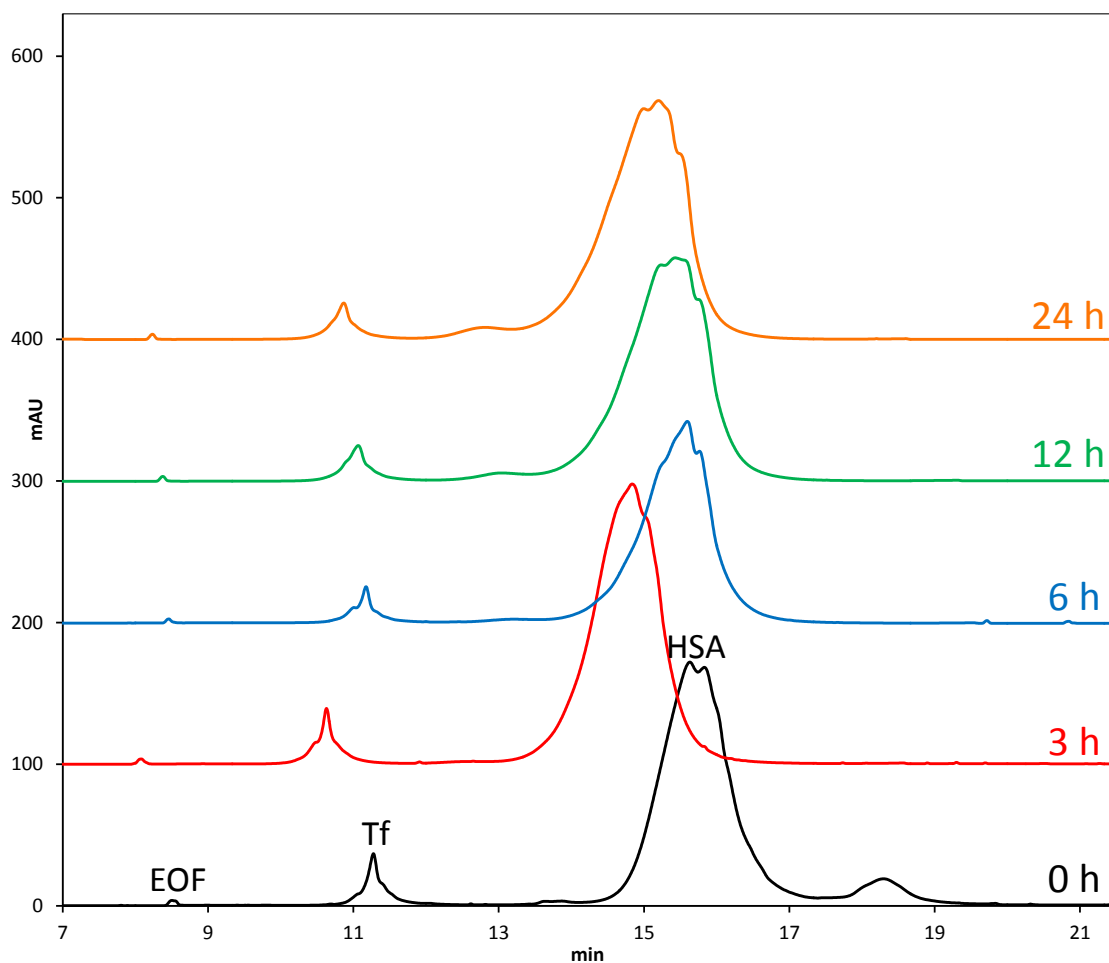
Figure 23 UV-Electropherograms of sequential runs of HSA/Tf mixture with a HPC coated capillary (70 cm total length, 50 µm i.d.). Sample tray temperature 37 °C, BGE: 100 mM NH_4HCO_3 pH 7.9, -30 kV.

In summary, capillary coatings providing cationic, anionic and neutral surfaces were tested to separate Tf and HSA isoforms. A BGE of 25 mM NH_4HCO_3 pH 8.5 was used in case of charged capillary surfaces, 100 mM NH_4HCO_3 pH 7.9 gave the best results in case of neutral surfaces (Table 2).

Table 2 Final BGE concentrations, pH and separation voltages employed for the different coatings.

| | BGE | | |
	NH_4HCO_3 [mmol/L]	pH	separation voltage [kV]
fused silica	25	8.5	20
DS	25	8.5	20
PAMPS	25	8.5	20
Pluronic	100	7.9	-30
HPC	100	7.9	-30

Table 3 gives an overview of the results of the method development by CE–UV experiments. On a bare fused silica capillary as a starting point, HSA and Tf could be separated into two peaks but a separation of the isoforms was not feasible. A positively charged capillary surface provided by a cationic polyelectrolyte increased the protein/surface attraction resulting in one single peak, tailing and even baseline shift. Layer coatings with PDADMAC as interlayer and either DS or PAMPS as terminal layer providing a negative surface charge gave better results. With these, the EOF was reduced in comparison to the bare fused silica capillary. The Tf peak showed a beginning separation of the lower abundant isoforms from the major one indicated by broad signal boundaries and three shoulders in the peak. The shape of the later migrating HSA peak suggests a beginning isoform separation into two poorly resolved peaks. With the polyelectrolytes DS and PAMPS as anionic coating layers the isoform separation was similar. However, the PAMPS coating provided better stability with respect to migration times and mobilities over sequential runs indicated by lower RSD values.

Table 3 Average mobilities of EOF, Tf and HSA (highest intensity) with RSDs, number of (partly) separated peaks and number of successive electrophoretic runs (n) in CE–UV experiments.

	μ_{EOF} [$10^{-4}cm^2V^{-1}s^{-1}$]	RSD [%]	μ_{Tf} [$10^{-4}cm^2V^{-1}s^{-1}$]	RSD [%]	peaks Tf	μ_{HSA} [$10^{-4}cm^2V^{-1}s^{-1}$]	RSD [%]	peaks HSA	n
fused silica	6.35	1.17	5.35	1.20	1	4.44	1.30	1	2
DS	3.94	1.39	2.88	2.21	4	1.89	3.82	2	33
PAMPS	4.31	0.50	3.24	0.36	4	2.27	0.36	2	33
Pluronic	-	-	-0.82	1.33	6	-1.69	1.06	3	29
HPC	-	-	-0.74	8.69	6	-1.59	3.47	3	13

The coatings that provided a neutral surface, *i.e.* pluronic and HPC, showed good results in case of isoform separation for both proteins in a similar extent. The HSA peak could be distinguished into three species; Tf separated even into 6 isoforms. While the resolution of HSA was slightly better with the HPC coating, the pluronic coating was more stable.

5.2 Interaction of HSA/Tf with Cisplatin by CE–UV

The coatings with the most promising results were chosen for incubation with cisplatin, namely the 4-layer coatings PDADMAC/DS and PDADMAC/PAMPS and the neutral pluronic coating. The protein solution (4 mM phosophates, 25 mM carbonates, 100 mM sodium chloride, Tf/HSA mixture under near-physiological concentrations of 30 and 600 µM, respectively) was mixed with cisplatin in a 1 : 1 ratio to HSA, *i.e* 600 µM. The sample vial was incubated at 37 °C in the sample tray immediately after preparation.

5.2.1 Dextran sulfate as terminal coating

Migration time shifts to longer times were observed over 24 h (Figure 24) with a 4-layer PDADMAC/DS coating, similarly to the protein mixture without cisplatin (Figure 14). Accordingly, in the first run (0 h) the HSA peak showed a partial separation into two peaks. Over time, however, additional but unresolved signals appeared in front of the HSA peak and increased over time, which indicate platination of the protein. Cisplatin can provide a positive charge and compensate a negative charge of the protein when binding to it. Consequently, the magnitude of the effective mobility of an anionic protein decreases when it is platinated. The apparent mobility is the sum of the EOF mobility and the effective mobility of the analyte which is negative for anions. This results in a higher apparent mobility and an earlier migration time. Moreover, two smaller and broader peaks can be observed that significantly migrate before and after the HSA peak. The signal with lower mobility was also observed in the runs without cisplatin, and thus, was not assigned to a platinated protein.

The peak shape of Tf also changed over time. A small shoulder increased at the front of the peak, while at the same time, the signal for the tetrasialo-Tf seems to decrease slightly. This indicates Tf platination. Interestingly, the shoulder decreases again over time. This might indicate that cisplatin forms only temporary adducts with Tf (average μ_{EOF}=4.04·10^{-4} cm^2 V^1 s^{-1}, RSD 2.95%, average μ_{Tf}=2.99·10^{-4} cm^2 V^{-1} s^{-1}, RSD 2.86%, average μ_{HSA}=2.02·10^{-4} cm^2 V^{-1} s^{-1}, RSD 2.98%, n=33).

Figure 24 UV-electropherograms of sequential runs of HSA/Tf/Cisplatin mixture with a 4-layer coated capillary (70 cm total length, 50 μm i.d.) with DS as terminal layer. Sample tray temperature 37 °C, BGE: 25 mM NH$_4$HCO$_3$ pH 8.5, 20 kV.

5.2.2 Poly(2-acrylamido-2-methyl-1-propanesulfonic acid) as terminal coating

Figure 25 shows selected runs of the transferrin/albumin mixture with cisplatin in a 1 : 1 molar ratio to HSA and with a 4-layer coating with PAMPS as the terminal layer. Migration time shifts are apparent. The shift in the red electropherogram after 3 h incubation might indicate that a protein was not detached from the coated capillary surface before the subsequent run. However, the overall migration time shifts are still negligible with respect to the RSD of the mobilities (average μ_{EOF}=4.28·10^{-4} cm^2 V^{-1} s^{-1}, RSD 1.71%, average μ_{Tf}=3.24·10^{-4} cm^2 V^{-1} s^{-1}, RSD 2.17%, average μ_{HSA}=2.33·10^{-4} cm^2 V^{-1} s^{-1}, RSD 3.27%, n=33).

The peak shape of the transferrin signal clearly differs from the metal complex-free sample, and shows similar characteristic compared to the DS coating. The HSA peak partly splits into 4 peaks and an additional smaller peak at an earlier migration time is visible.

Figure 25 UV-Electropherograms of sequential runs of a HSA/Tf/Cisplatin mixture with a layer coated capillary (70 cm total length, 50 μm i.d.) with PAMPS as terminal layer. Sample tray temperature 37°C, BGE: 25 mM NH$_4$HCO$_3$ pH 8.5, 20 kV.

In comparison to the DS coating, the PAMPS coating seems to provide higher coating stability as the migration times show better consistency. This might be explained by decreased interactions of the PAMPS polymer with the proteins causing less protein adsorption. However, with respect to the resolution of the interaction products, both the DS and PAMPS coating delivered comparable results. It seems that cisplatin forms adducts with both proteins, but only transiently with Tf. The free thiol is probably the most efficient in coordinating cisplatin.

5.2.3 Pluronic coated capillary

The pluronic coated capillary provides a neutral surface (average μ_{Tf}=-0.82·10^{-4} cm^2 V^{-1} s^{-1}, RSD 1.06%, average μ_{HSA}=-1.69·10^{-4} cm^2 V^{-1} s^{-1}, RSD 1.33%, n=29). The first separation run, directly after preparing the sample solution did not show any difference to the electropherograms of the sample without cisplatin (Figure 26, Figure 21). After 3 h incubation, additional HSA peaks with

longer migration times (red track) indicate the formation of multiple platinated species. While the major peak, mostly native HSA, decreased over time, the platinated HSA peaks increased (compare 0 h (black), 3 h (red) and 6 h (blue) track). The case of Tf platination is less obvious. Di- and trisialo-Tf peaks seem to be increased in the red track on the right hand side of Figure 26 in comparison to the experiments without cisplatin (Figure 21) and might indicate overlapping peaks of platinated Tf species. However, these signals decrease again over time similarly to the finding from the negatively charged coatings indicating that HSA is the preferred interaction partner under these near-physiological conditions.
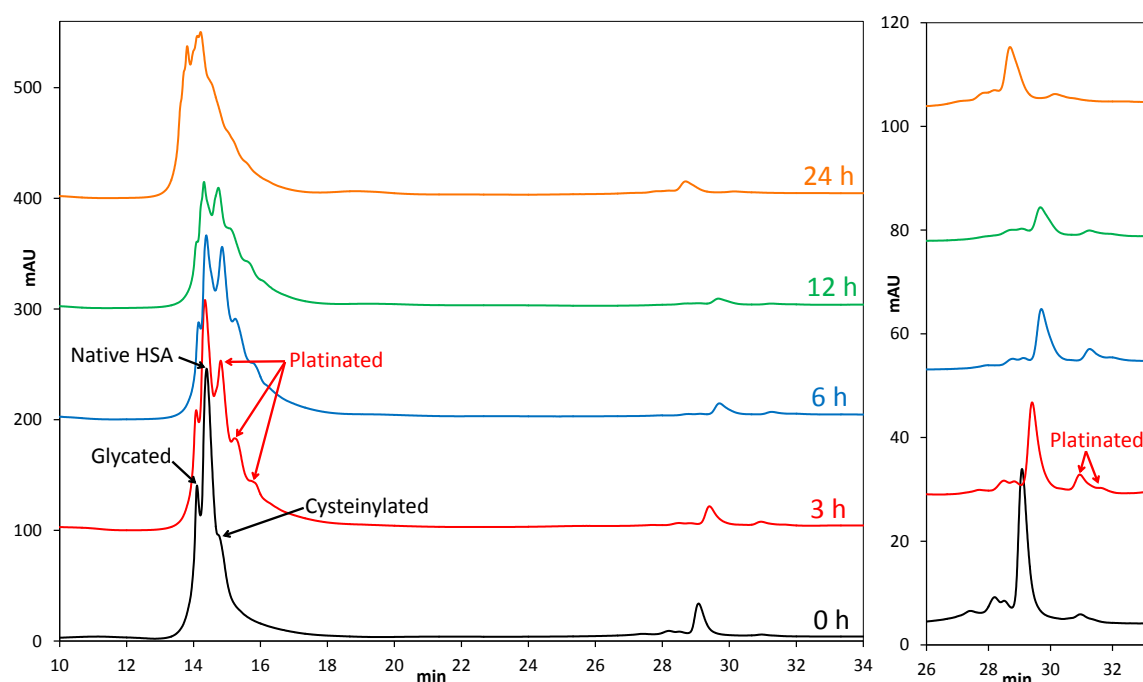
Figure 26 UV-Electropherograms of sequential runs of a HSA/Tf/Cisplatin mixture with a pluronic coated capillary (70 cm total length, 50 µm i.d.). Enlarged section of Tf peaks on the right hand side. Sample tray temperature 37 °C, BGE: 100 mM NH_4HCO_3 pH 7.9, -30 kV.

5.3 Identification of Tf and HSA microheterogeneity by ESI-TOF MS

Identical Tf and HSA, compared to the previous experiments, were used for the MS-studies. Tf was dissolved in water in a concentration of 100 µM for a first ESI-TOF (time-of-flight) MS experiment. This solution was diluted 1:10 with methanol/water (50:50 (v/v), 2% formic acid) prior to injection into the mass spectrometer and the sample was analyzed in the positive ion mode. Figure 27A presents the full mass profile over a range of 1500–3000 m/z observed for a Tf infusion. The eight most prominent peaks are charged between $z = 31+$ and 38+. The enlargement of the most abundant 35+ and the second most abundant peak 34+ (Figure 27B) reveals the microheterogeneity of the Tf sample, which is due to post-translational modifications. The mass spectrum was deconvoluted with the maximum entropy deconvolution algorithm using automatic data point spacing, 30 000 resolving power and without smoothing (Figure 27C). The high charge states do not allow the detection of isotopic distributions despite the high resolving power. Some of the Tf glycoforms were identified. The most abundant peak at 79553.68 Da was assigned to the tetrasialo-Tf (m_{theor} = 79553.14 Da) in accordance with CE-UV experiments. Trisialo-Tf at 79262.33 Da (m_{theor} = 79260.88 Da) and pentasialo-Tf at 80206.82 Da (m_{theor} = 80209.74 Da) were also observed but with much lower intensities. Additionally, two other peaks were assigned to tetrasialo-Tf isoforms, one with an additional GlcNAc at 79742.42 Da (m_{theor} = 79756.34 Da). The second peak was assigned with an oxidized form with additional GlcNAc and Man at 79934.58 Da (m_{theor} = 79934.48 Da) (Table 4). The 2- and 6-sialo isoforms of Tf were not detectable. The found masses are in good accordance with the theoretical values. However, the peak identification of the MS detection could not be confirmed with absolute certainty, because standards of each glycoform were not available.
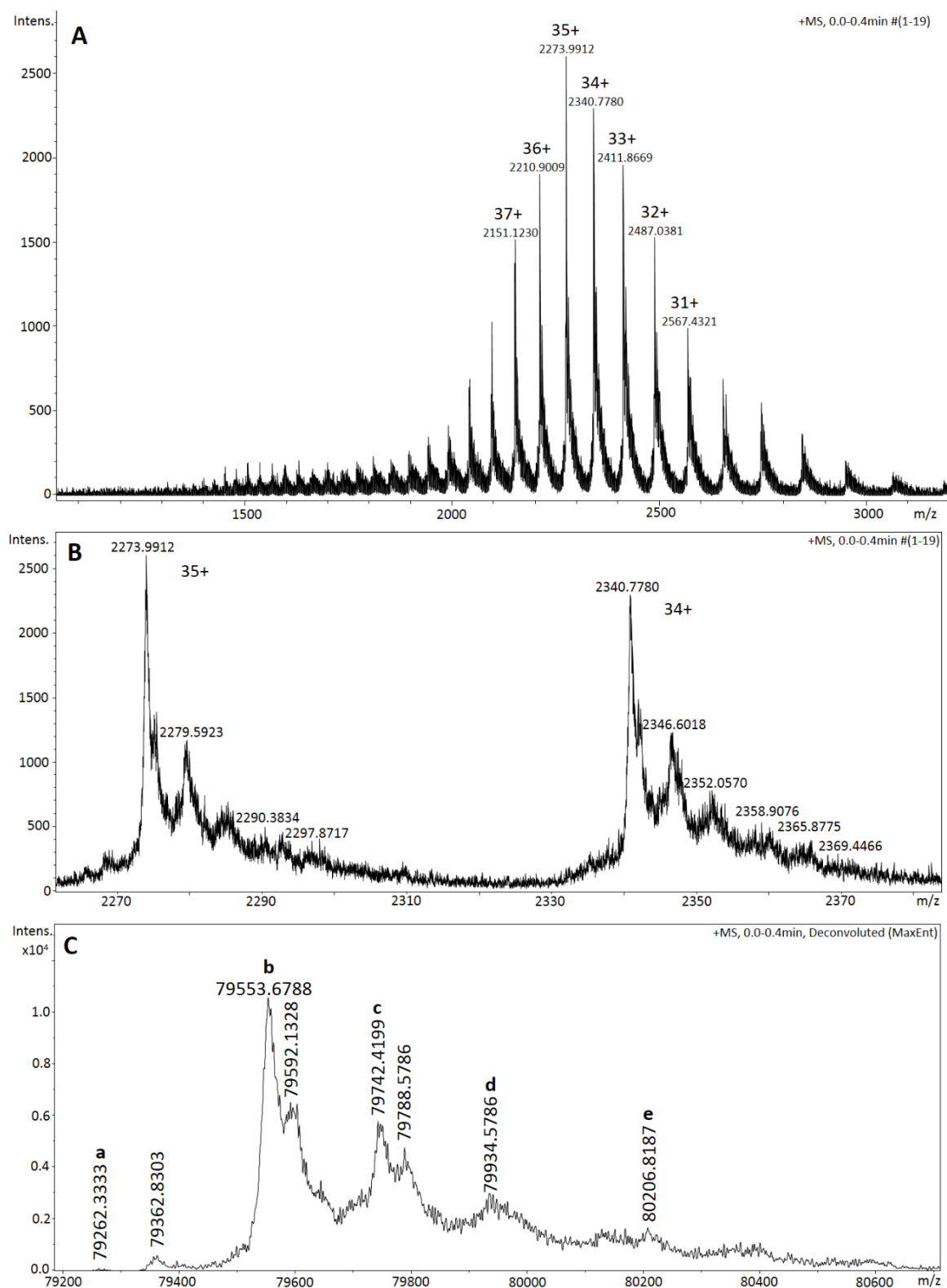
Figure 27 ESI-TOF-MS of Tf by direct infusion. (A) The full mass spectrum observed for Tf shows multiple charge states. The 35+ peak shows the highest intensity. (B) Enlarged section displaying the 35+ and 34+ charged peaks. (C) Deconvoluted mass spectrum showing the microheterogeneity of Tf sample in a 1+ charge state (peak assignment in Table 4).

Figure 28A shows the MS profile of HSA in a range of approx. 1100-2500 m/z. HSA is found in many charge states where the 43+ form shows the highest intensity. Four of the peaks in the deconvoluted mass spectrum (Figure 28B) could be assigned to HSA isoforms (Table 4). The native HSA at 66437.24 Da (m_{theor} = 66438.27 Da) is partly overlapped with a neighboring peak that most likely indicates a nitrosylated form (m_{theor} = 66468.27 Da). The peak with the highest intensity at 66556.71 Da refers to HSA with a Cys34 building a disulfide bridge with a single Cys (m_{theor} = 66557.41 Da). The neighboring peak at 66599.43 Da indicates glycated HSA (m_{theor} = 66600.41 Da). The mass found at 66718.06 Da can be associated with cysteinylated and glycated HSA (m_{theor} = 66719.55 Da).
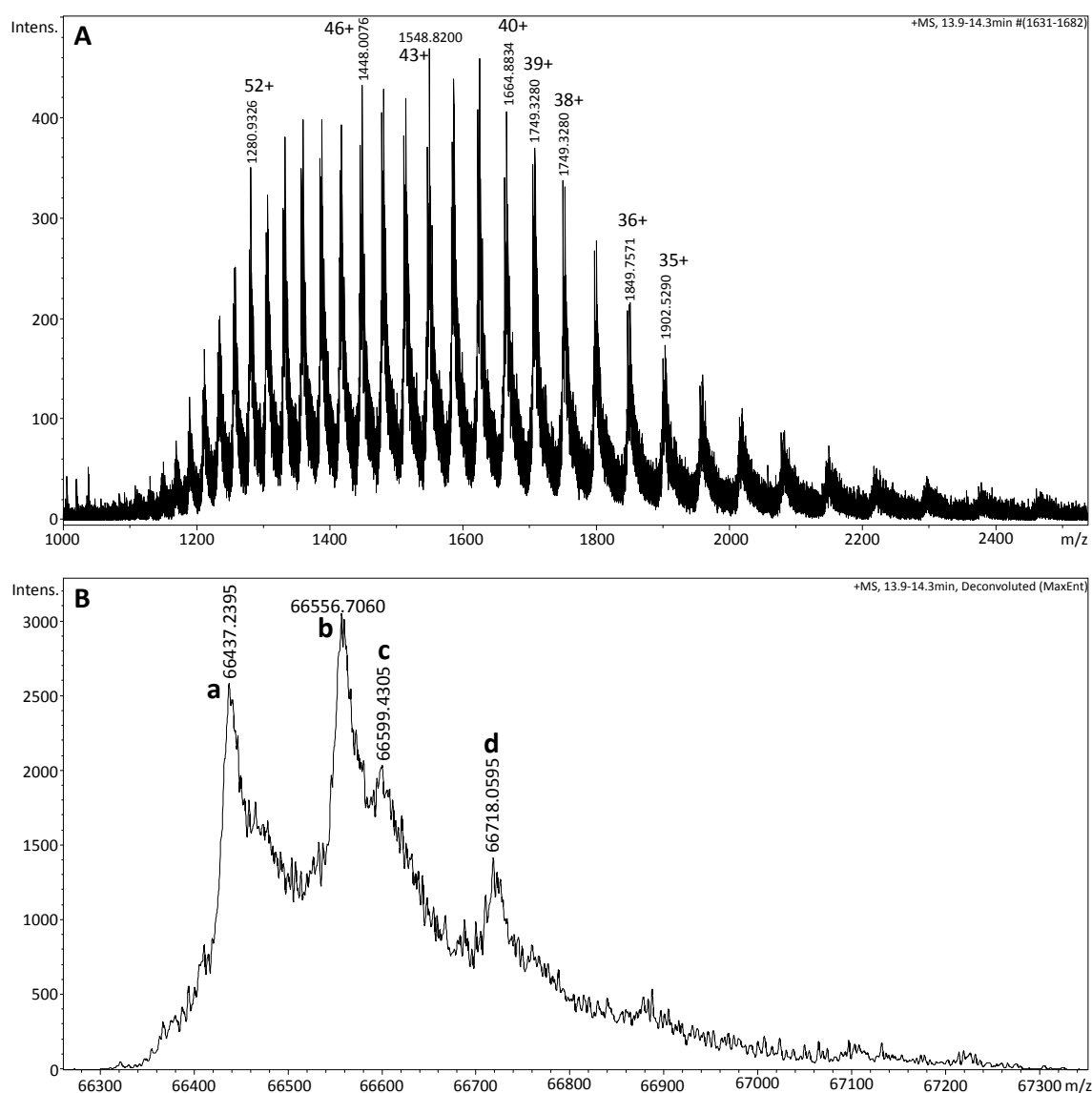
Figure 28 Results with CE–ESI-TOF-MS for injection of HSA/Tf mixture on a PDADMAC/PAMPS coated capillary. (A) MS profile observed for HSA with multiple charge states. The 43+ peak shows the highest intensity. (B) Deconvoluted mass spectrum displaying the micro-heterogeneity of HSA (peak assignment in Table 4).

Table 4 Assignment of the deconvoluted mass signals to Tf isoforms in Figure 27C (27a–27e) and of HSA isoforms from Figure 28B (28a–28d).

Peak	Form	mass (Da)	
		theoretical [M+H]$^+$	found
27**a**	3-sialo Tf	79260.88	79262.33
27**b**	4-sialo Tf	79553.14	79553.68
27**c**	4-sialo Tf+GlcNAc	79756.34	79742.42
27**d**	4-sialo Tf+GlcNAc+Man+O	79934.48	79934.58
27**e**	5-sialo-Tf	80209.74	80206.82
28**a**	native HSA	66438.27	66437.24
28**b**	HSA + Cys	66557.41	66556.71
28**c**	HSA + Hexose	66600.41	66599.43
28**d**	HSA + Cys + Hexose	66719.55	66718.06

Again, the lack of availability of a standard of each HSA isoform does not allow identifying the peaks with absolute certainty.

5.4 CE–ESI-TOF-MS

Two capillary coatings providing a negatively charged surface, namely the 4-layer coatings PDADMAC/DS and PDADMAC/PAMPS, and one neutral coating based on the pluronic polymer, were tested in CE experiments hyphenated to MS. The instruments were coupled using a coaxial sheath-flow ESI interface from Agilent Technologies. During initial analysis of the HSA/Tf mixture by CE–MS using the conventional hydrodynamic injection (20 mbar, 5 s) no peaks assignable to proteins were observed in the MS. Therefore, a larger injection plug was necessary for further experiments to increase the protein concentrations (50 mbar, 30 s), which was also noted in the literature [118].

The total ion current electropherograms (TIE) of DS coated capillaries showed only one broad signal for the proteins with a complete loss of resolution (Figure 29). This was also observed by online UV detection prior the introduction into the mass spectrometer (Figure 30). Suction effects caused by the nebulizing gas may be a possible explanation for this observation. Another factor might be the composition difference between the sheath liquid (methanol-water 50:50 (v/v), 2% formic acid) and the BGE (25 mM NH_4HCO_3 pH 8.5). Ions from the BGE can diffuse to the sheath liquid and ions from the sheath liquid go into the capillary because of concentration differences and cause widening of the electrophoretic peaks [117]. In addition to the poor resolution the TIE also shows many spikes that indicate a poor ESI spray.
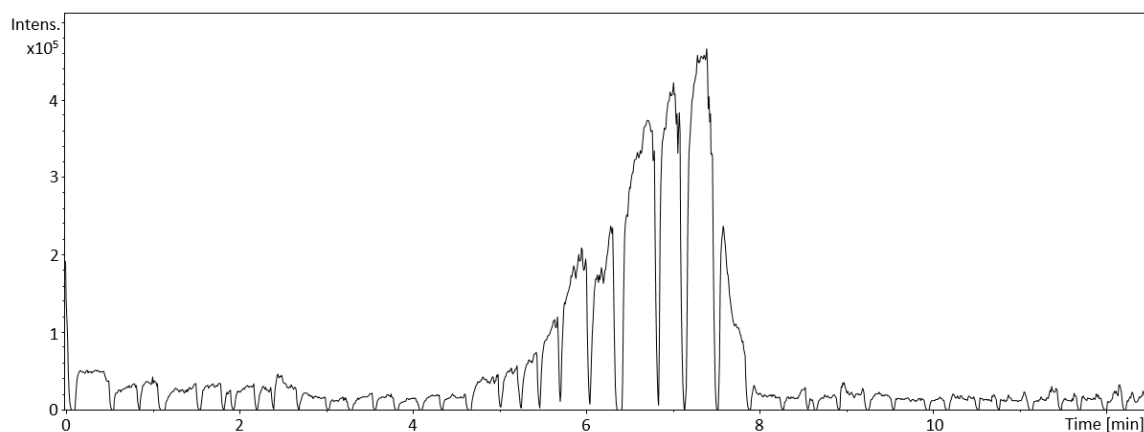
Figure 29 Total ion current electropherogram (TIE). CE–ESI-TOF-MS experiments of a HSA/Tf mixture on a PDADMAC/DS coated capillary (70 cm total length, 50 µm i.d.). Injection: 50 mbar 30 s, BGE: 25 mM NH_4HCO_3 pH 8.5, separation voltage: 30 kV, sheath liquid: methanol-water 50:50 (v/v), 2% formic acid.
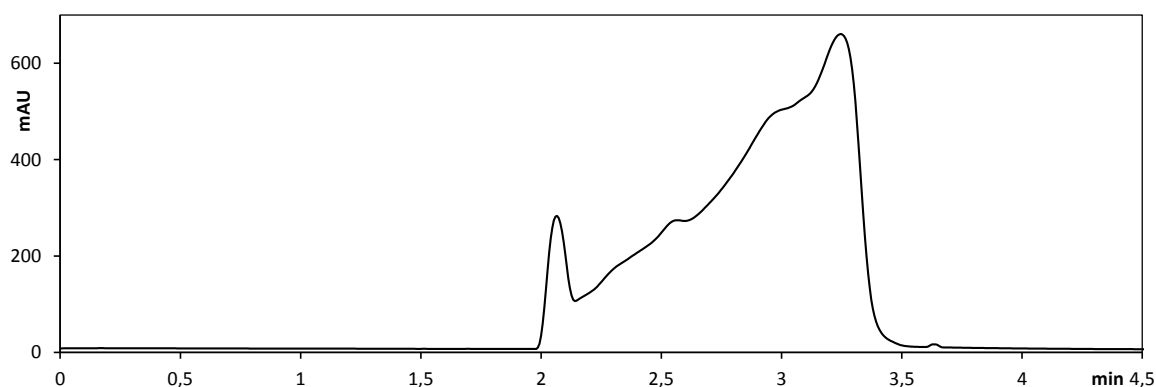
Figure 30 UV-Electropherogram. CE–ESI-TOF-MS experiments of a HSA/Tf mixture on a PDADMAC/DS coated capillary (70 cm total length, 50 µm i.d.). UV detection at 27 cm, other conditions see Figure 29.

The UV track of an analysis on a capillary with PAMPS as terminal coating layer is shown in Figure 31. There is a separation of the smaller Tf (between 3.5 min and 4 min) from the bigger HSA peak (between 4.5 min and 8 min.
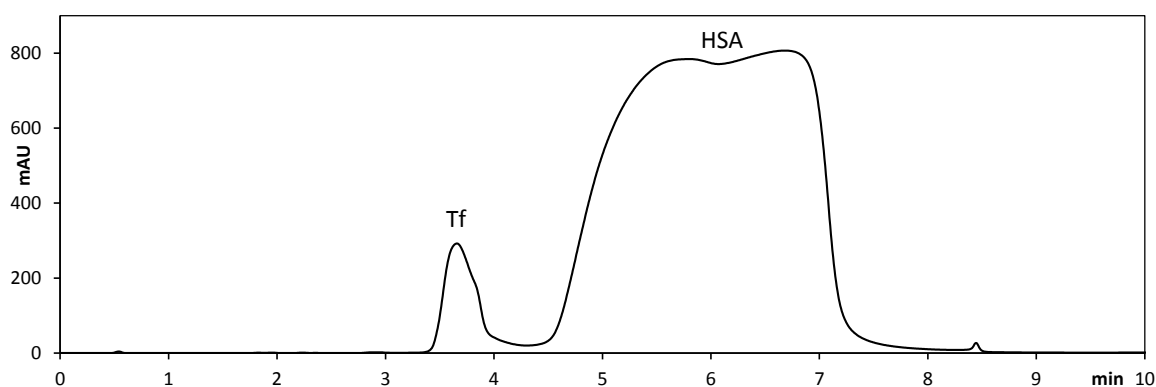
Figure 31 UV-Electropherogram. CE–ESI-TOF-MS experiments of a HSA/Tf mixture on a PDADMAC/PAMPS coated capillary (70 cm total length, 50 µm i.d.). Injection: 50 mbar 30 s, BGE: 25 mM NH_4HCO_3 pH 8.5, separation voltage: 24 kV, UV detection at 27 cm, sheath liquid: methanol-water 50:50 (v/v), 2% formic acid.

Figure 32 shows extracted-ion electropherograms (EIE) of the most abundant HSA and Tf molecule ion on a PAMPS coated capillary. The EIEs indicate a separation between a small Tf peak (approx. 9.5–11 min) and a big HSA peak (approx. 12–18 min). However, no isoform separation is visible. The increase of the EIE of Tf during the HSA peak is probably caused by an increased background due to HSA signals. Note the intensity scales of the proteins.
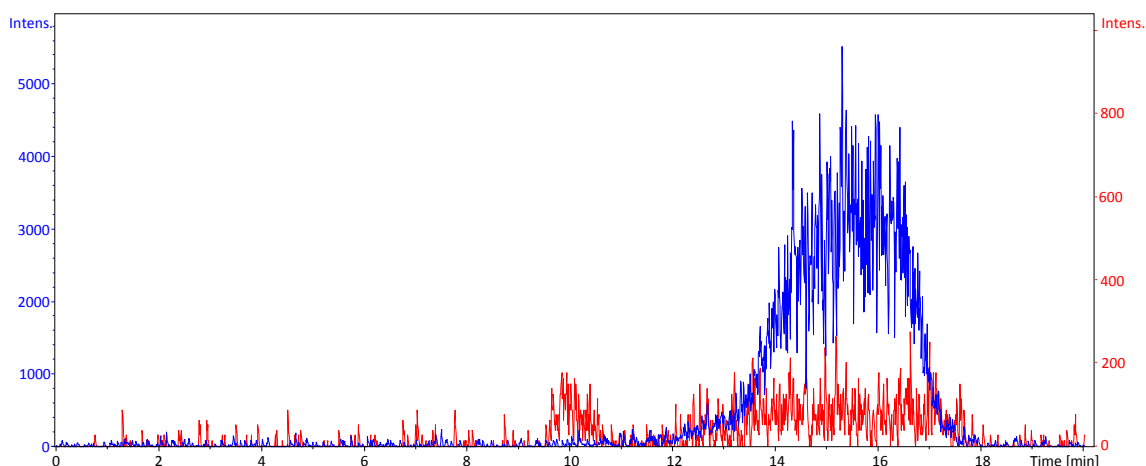
Figure 32 Extracted-ion electropherograms (EIE). CE–ESI-TOF-MS experiments of a HSA/Tf mixture on a PDADMAC/PAMPS coated capillary (70 cm total length, 50 µm i.d.). Injection: 50 mbar 30 s, BGE: 25 mM NH_4HCO_3 pH 8.5, separation voltage: 24 kV, sheath liquid: methanol-water 50:50 (v/v), 2% formic acid. Blue track: EIE of most abundant HSA ion (1548.9±0.3 *m/z*). Red track: EIE of most abundant Tf ion (2276.0±0.3 *m/z*).

Despite the poor separation, the proteins were detectable by ESI-MS. The intensity of the Tf signal was very low. The mass with the highest abundance in the deconvoluted mass spectrum was at 79603.00 Da (Figure 33) most probably corresponding to the 4-sialo-Tf.
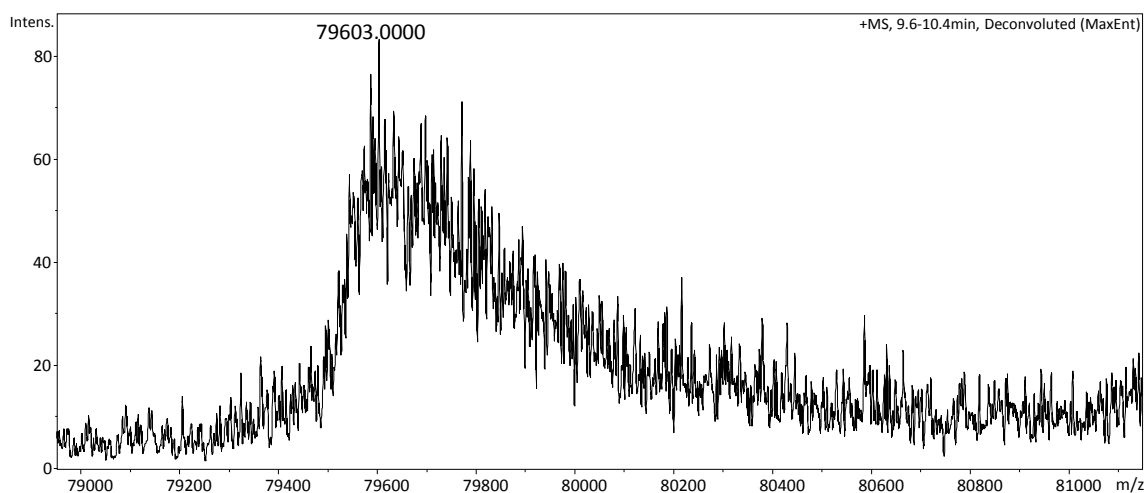
Figure 33 Deconvoluted mass spectrum of Tf with MaxEnt of CE–ESI-TOF-MS for HSA/Tf injection.

The neutral Pluronic coating does not produce an EOF that would provide a bulk flow to the capillary outlet. However, a bulk flow is essential to deliver the analytes to the ion source and to provide a stable ESI spray. In order to compensate the missing EOF a continuous pressure of 50 mbar was applied during the analysis. A signal was detected with the online UV detection

(Figure 34) but no peak was observed in the total ion current electropherogram of the mass spectrometer. ESI spray instabilities are also an issue with pluronic coated capillaries.
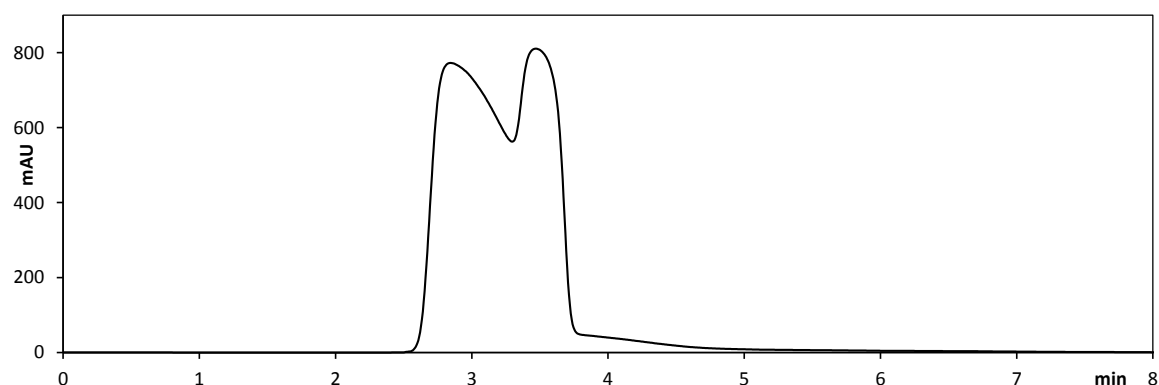
Figure 34 UV-Electropherogram. CE–ESI-TOF-MS experiments of a HSA/Tf mixture on a pluronic coated capillary (70 cm total length, 50 µm i.d.). Injection: 50 mbar 30 s, BGE: 100 mM NH_4HCO_3 pH 7.9, separation voltage: 30 kV, continuous pressure 50 mbar, UV detection at 27 cm, sheath liquid: methanol-water 50:50 (v/v), 2% formic acid.

When injecting a 5 day old sample of the HSA/Tf mixture, the Tf peak with a maximum at approx. 12.2 min is clearly visible and separated from the HSA peak (Figure 35).
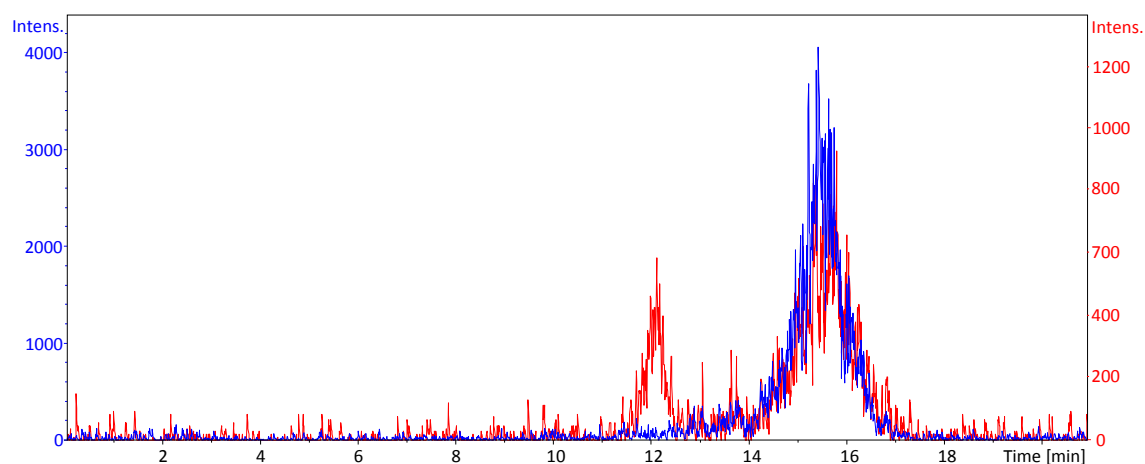
Figure 35 Extracted-ion electropherograms (EIE). CE–ESI-TOF-MS experiments of a 5 days old HSA/Tf mixture on a PDADMAC/PAMPS coated capillary (70 cm total length, 50 µm i.d.). Injection: 50 mbar 30 s, BGE: 25 mM NH_4HCO_3 pH 8.5, separation voltage: 24 kV, sheath liquid: methanol-water 50:50 (v/v), 2% formic acid. Blue track: EIE of HSA ion with high abundance (1578.9±0.3 *m/z*). Red track: EIE of most abundant Tf ion (2276.0±0.3 *m/z*).

Many *C*-terminal truncated HSA forms could be identified in the MS as indicated by Figure 36. This clearly demonstrates the importance of using freshly prepared protein samples. The enlarged section of the 42+ and 41+ peaks reveals the degradation of HSA (Figure 36B), and is

59

even more evident in the deconvoluted mass spectrum (Figure 36C). Additional to the native, cysteinylated and glycated HSA forms, peaks were found that could be assigned to truncated HSA and the loss of up to seven amino acids at the *C*-terminus by hydrolysis (Figure 36 and Table 5). Although Chan *et al.* suggest that about 25% of circulating HSA has the first two *N*-terminal amino acids, *i.e.* aspartic acid (D) and alanine (A), cleaved off (m_{theor} = 66241.01 Da), no peak could be assigned in the mass spectra of either the fresh sample or the aged sample [36].
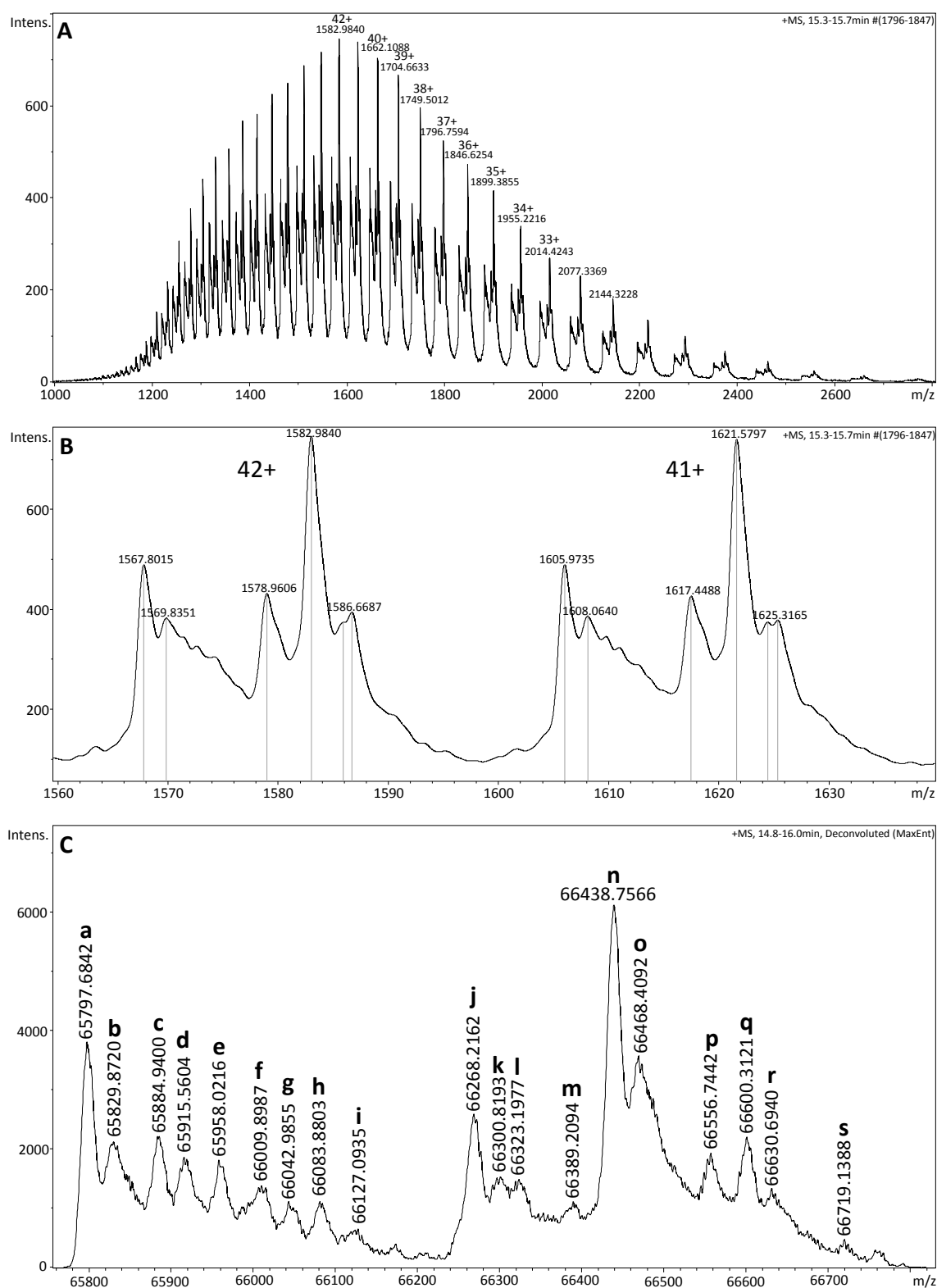
Figure 36 Results with CE–ESI-TOF-MS for 5 day old HSA/Tf injection on a PDADMAC/PAMPS coated capillary. (A) MS spectrum observed for HSA with multiple charge states. 42+ peak shows the highest intensity. (B) Enlarged section: 42+ and 41+ charged peaks. (C) Deconvoluted mass spectrum of HSA displaying many truncated forms (peak assignment in Table 5).

61

Table 5 Experimental mass values obtained by on-line CE–ESI-MS analysis of HSA/Tf mixture stored 5 days at RT. Assignment of the deconvoluted mass signals to HSA isoforms in Figure 36C.

Peak	Form	mass [Da] theoretical mass $[M+H]^+$	found mass
a	HSA - SQAALGL	65797.54	65797.68
b	HSA-SO$_2$H - SQAALGL	65829.54	65829.87
c	HSA - QAALGL	65884.61	65884.94
d	HSA - SQAALGL + Cys	65916.68	65915.56
e	HSA - SQAALGL + Hexose	65959.68	65958.02
f	HSA - AALGL	66012.74	66009.90
g	HSA-SO$_2$H - AALGL	66044.74	66042.99
h	HSA - ALGL	66083.82	66083.88
i	HSA - AALGL + Cys	66131.89	66127.09
j	HSA - GL	66268.06	66268.22
k	HSA-SO$_2$H - GL	66300.06	66300.82
l	HSA - L	66325.11	66323.20
m	HSA - GL + Cys	66387.20	66389.21
n	native HSA	66438.27	66438.76
o	HSA-SNO	66468.27	66468.41
p	HSA + Cys	66557.41	66556.74
q	HSA + Hexose	66600.41	66600.31
r	HSA-SNO + Hexose	66630.41	66630.69
s	HSA + Cys + Hexose	66719.55	66719.14

The intensity of Tf was very low. Only the most abundant tetrasialo form (m_{theor} = 79553.14 Da) could be assigned to the found mass of 79556.99 Da in the deconvoluted spectrum (Figure 37).
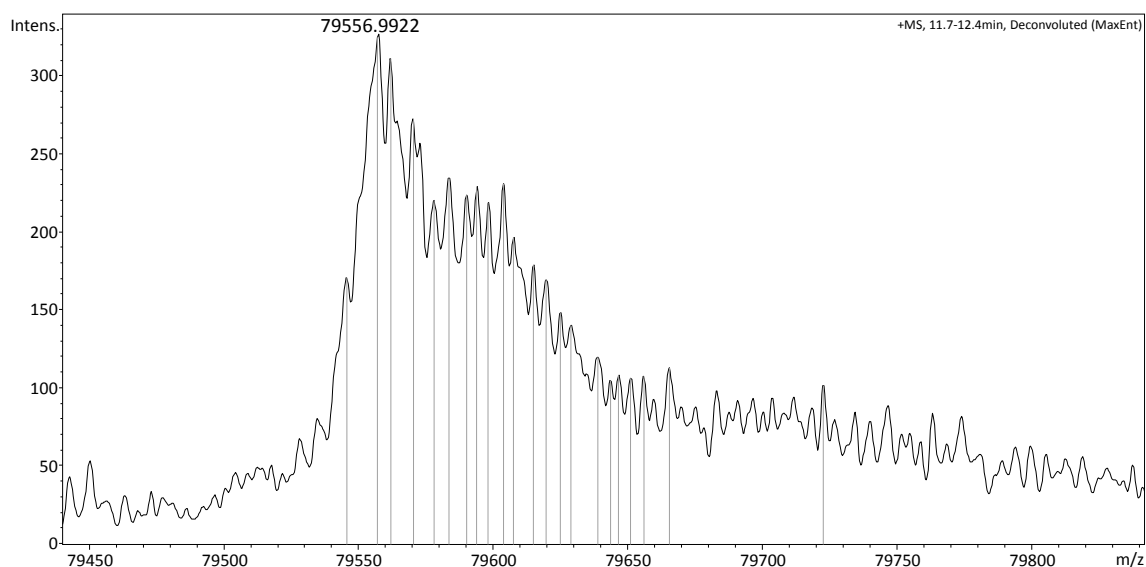
Figure 37 Deconvoluted mass spectrum of Tf with MaxEnt of CE–ESI-TOF-MS for 5 day old HSA/Tf injection.

The reaction of cisplatin with the HSA/Tf mixture was not investigated by CE–MS due to the poor resolution of the isoforms.

6 Conclusion and outlook

This master thesis is focused on the separation of intact human serum albumin and transferrin isoforms by capillary electrophoresis under ESI-MS compatible conditions and the interaction of these proteins with cisplatin.

Several capillary coatings were investigated with the aim to reduce the protein/capillary surface interactions and to modify the EOF in a way to obtain high resolution for separating the isoforms. Mixtures of HSA/Tf under near physiological conditions and in physiological concentrations with and without addition of cisplatin have been studied.

A pluronic coating providing a neutral capillary surface showed the best results in the CE–UV mode with respect to coating stability and isoform separation of HSA and Tf. HSA was partially separated into 3 isoforms, while for Tf even 6 isoforms were distinguishable. Several of these protein isoforms were identified by ESI-TOF-MS experiments by direct infusion. A total of 5 masses found were matching with Tf isoforms, namely trisialo-Tf, tetrasialo-Tf, pentasialo-Tf and two variants of tetrasialo-Tf. In case of HSA the native, cysteinylated, glycated and a both cysteinylated and glycated form were identified. The MS data supports the findings by CE–UV experiments.

In case of the CE–MS measurements, the intensity of Tf in the mass spectrum was very low and only the most abundant tetrasialo isoform was found despite the increased injection volume compared to CE–UV experiments. The HSA isoforms were well detectable during these experiments, but isoform resolution was lost. In an aged (5 days at RT) HSA/Tf sample mixture many truncated HSA isoforms with *C*-terminal loss of up to 7 amino acids could be identified in the MS.

However, when performing the CE–MS coupling with a pluronic coated capillary no peaks were observed in the MS even when applying a continuous pressure. A 4-layer coated capillary with PAMPS as negative charged terminal layer could separate HSA and Tf but any isoform resolution that was recognized in the CE–UV mode was lost.

In interaction experiments with cisplatin by CE–UV several platinated protein species were observed. Data from incubation experiments at 37 °C over 24 h with sequential electrophoretic runs suggest that cisplatin binds to both HSA and Tf but only transiently to Tf. The free thiol of HSA might be the most efficient coordination site for cisplatin.

This work highlights the challenges of CE–MS hyphenation, especially when investigating intact proteins and their interaction with metallodrugs. Future experiments might consider a sheathless interface as an alternative to the sheath-flow CE–MS interface to cope with the poor sensitivity since it works without dilution. Alternative materials for CE capillaries could be tested such as polyether ether ketones with reduced EOF and improved coating stability [130]. Alternative detectors to ESI-MS could give complementary information. Matrix assisted laser desorption/ionization-MS could be done in combination with an automated spotter in an offline mode [131]. Hyphenation with inductively coupled plasma-MS might be a powerful tool to determine metal binding to protein isoforms that is not limited to volatile separation buffers [9, 131]. Finally, binding studies with other compounds (*e.g.* ruthenium complexes) can be of interest.

List of Figures

List of Tables

List of Equations

References

1.   Barry, N.P. and P.J. Sadler, *Exploration of the medical periodic table: Towards new targets.* Chemical Communications, 2013. **49**(45): p. 5106-5131.

2.   Lokich, J. and N. Anderson, *Carboplatin versus cisplatin in solid tumors: An analysis of the literature.* Annals of Oncology, 1998. **9**(1): p. 13-21.

3.   Maeda, H., et al., *Tumor vascular permeability and the EPR effect in macromolecular therapeutics: a review.* Journal of Controlled Release, 2000. **65**(1–2): p. 271-284.

4.   Kratz, F., *Albumin as a drug carrier: Design of prodrugs, drug conjugates and nanoparticles.* Journal of Controlled Release, 2008. **132**(3): p. 171-183.

5.   Shields, S.J., et al., *Mass spectrometry and non-covalent protein-ligand complexes: confirmation of binding sites and changes in tertiary structure.* Journal of the American Society for Mass Spectrometry, 2003. **14**(5): p. 460-470.

6.   Heck, A.J.R., *Native mass spectrometry: a bridge between interactomics and structural biology.* Nature Methods, 2008. **5**(11): p. 927-933.

7.   Qian, J., et al., *Development of a high performance size exclusion chromatography method to determine the stability of Human Serum Albumin in a lyophilized formulation of Interferon alfa-2b.* Journal of Chromatography A, 2008. **1194**(1): p. 48-56.

8.   Hayashi, T., et al., *The importance of sample preservation temperature for analysis of the redox state of human serum albumin.* Clinica Chimica Acta, 2002. **316**(1–2): p. 175-178.

9.   Arizaga Rodríguez, S., et al., *Detection of transferrin isoforms in human serum: comparison of UV and ICP–MS detection after CZE and HPLC separations.* Analytical and Bioanalytical Chemistry, 2005. **383**(3): p. 390-397.

10.   Turell, L., et al., *HPLC separation of human serum albumin isoforms based on their isoelectric points.* Journal of chromatography. B, Analytical technologies in the biomedical and life sciences, 2014. **944**: p. 144-51.

11.   Anraku, M., et al., *Effect of Oxidative Stress on the Structure and Function of Human Serum Albumin.* Pharmaceutical Research, 2001. **18**(5): p. 632-639.

12.   Bar-Or, D., et al., *Heterogeneity and oxidation status of commercial human albumin preparations in clinical use.* Critical Care Medicine, 2005. **33**(7): p. 1638-1641.

13.   Hardt, M., et al., *Toward defining the human parotid gland salivary proteome and peptidome: identification and characterization using 2D SDS-PAGE, ultrafiltration, HPLC, and mass spectrometry.* Biochemistry, 2005. **44**(8): p. 2885-99.

14.   Bruce Alberts, A.J., Julian Lewis, Martin Raff, Keith Roberts, Peter Walker, *Molecular Biology of the Cell*. 5th ed 2007, New York: Garland Science.

15.   Eaton, P., *Clinical Biochemistry Reference Ranges Handbook*, 2013.

16.   Putnam, F.W., *1 - Progress in Plasma Proteins*. The Plasma Proteins (Second Edition), ed. F.W. Putnam 1984: Academic Press. 1-44.

17.   Peters Jr, T., *All about Albumin: Biochemistry, Genetics and Medical Applications*, ed. T. Peters Jr 1996, San Diego and London: Academic Press.

18.   Fanali, G., et al., *Human serum albumin: From bench to bedside.* Molecular Aspects of Medicine, 2012. **33**(3): p. 209-290.

19.   Sugio, S., et al., *Crystal structure of human serum albumin at 2.5 Å resolution.* Protein Engineering, 1999. **12**(6): p. 439-446.

20.   Oettl, K. and R.E. Stauber, *Physiological and pathological changes in the redox state of human serum albumin critically influence its binding properties.* British Journal of Pharmacology, 2007. **151**(5): p. 580-590.

21.   Jakubowski, H., *New method for the determination of protein N-linked homocysteine.* Analytical Biochemistry, 2008. **380**(2): p. 257-261.

22.   Brownlee, M., *The pathological implications of protein glycation.* Clinical and Investigative Medicine, 1995. **18**(4): p. 275-281.

23.   Ahmed, N., et al., *Peptide Mapping Identifies Hotspot Site of Modification in Human Serum Albumin by Methylglyoxal Involved in Ligand Binding and Esterase Activity.* Journal of Biological Chemistry, 2005. **280**(7): p. 5724-5732.

24.   Otagiri, M. and V.T.G. Chuang, *Pharmaceutically Important Pre- and Posttranslational Modifications on Human Serum Albumin.* Biological and Pharmaceutical Bulletin, 2009. **32**(4): p. 527-534.

25.   Lautenslager, G.T., et al., *Effects of nonenzymatic glycation and fatty acids on functional properties of human albumin.* Metabolism, 2011. **60**(12): p. 1683-1691.

26.   Sakata, N., A. Moh, and S. Takebayashi, *Contribution of superoxide to reduced antioxidant activity of glycoxidative serum albumin.* Heart and Vessels, 2002. **17**(1): p. 22-29.

27.   Van Campenhout, A., et al., *Iron-binding antioxidant capacity is impaired in diabetes mellitus.* Free Radical Biology and Medicine, 2006. **40**(10): p. 1749-1755.

28.   Rondeau, P. and E. Bourdon, *The glycation of albumin: Structural and functional impacts.* Biochimie, 2011. **93**(4): p. 645-658.

29.   Sampath, V., X.-J. Zhao, and W.S. Caughey, *Anesthetic-like Interactions of Nitric Oxide with Albumin and Hemeproteins: A MECHANISM FOR CONTROL OF PROTEIN FUNCTION.* Journal of Biological Chemistry, 2001. **276**(17): p. 13635-13643.

30.   Kashiba-Iwatsuki, M., M. Miyamoto, and M. Inoue, *Effect of Nitric Oxide on the Ligand-Binding Activity of Albumin.* Archives of Biochemistry and Biophysics, 1997. **345**(2): p. 237-242.

31.   Reuter, S., et al., *Oxidative stress, inflammation, and cancer: How are they linked?* Free Radical Biology and Medicine, 2010. **49**(11): p. 1603-1616.

32. Bourdon, E., et al., *Differential effects of cysteine and methionine residues in the antioxidant activity of human serum albumin.* Free Radical Research, 2005. **39**(1): p. 15-20.

33. Sadler, P.J., A. Tucker, and J.H. Viles, *Involvement of a lysine residue in the N-terminal Ni^{2+} and Cu^{2+} binding site of serum albumins.* European Journal of Biochemistry, 1994. **220**(1): p. 193-200.

34. Blindauer, C.A., et al., *Structure, Properties, and Engineering of the Major Zinc Binding Site on Human Albumin.* Journal of Biological Chemistry, 2009. **284**(34): p. 23116-23124.

35. Sokołowska, M., et al., *Spectroscopic and thermodynamic determination of three distinct binding sites for Co(II) ions in human serum albumin.* Journal of Inorganic Biochemistry, 2009. **103**(7): p. 1005-1013.

36. Chan, B., et al., *Site-specific N-terminal Auto-degradation of Human Serum Albumin.* European Journal of Biochemistry, 1995. **227**(1-2): p. 524-528.

37. Shaw, C.F., *The Protein Chemistry of Antiarthritic Gold(I) Thiolates and Related Complexes.* Comments on Inorganic Chemistry, 1989. **8**(6): p. 233-267.

38. Ivanov, A.I., et al., *Cisplatin Binding Sites on Human Albumin.* Journal of Biological Chemistry, 1998. **273**(24): p. 14721-14730.

39. Talib, J., J. Beck, and S. Ralph, *A mass spectrometric investigation of the binding of gold antiarthritic agents and the metabolite $[Au(CN)_2]^-$ to human serum albumin.* Journal of Biological Inorganic Chemistry, 2006. **11**(5): p. 559-570.

40. Shen, X.-C., et al., *Studies on the interaction between Ag^+ and human serum albumin.* Journal of Inorganic Biochemistry, 2003. **95**(2–3): p. 124-130.

41. Li, Y., et al., *Human Serum Albumin−Mercurial Species Interactions.* Journal of Proteome Research, 2007. **6**(6): p. 2277-2286.

42. Stewart, A.J., et al., *Interdomain zinc site on human albumin.* Proceedings of the National Academy of Sciences, 2003. **100**(7): p. 3701-3706.

43. Sadler, P.J. and J.H. Viles, *1H and 113Cd NMR Investigations of Cd^{2+} and Zn^{2+} Binding Sites on Serum Albumin: Competition with Ca^{2+}, Ni^{2+}, Cu^{2+}, and Zn^{2+}.* Inorganic Chemistry, 1996. **35**(15): p. 4490-4496.

44. Bal, W., et al., *Multi-metal binding site of serum albumin.* Journal of Inorganic Biochemistry, 1998. **70**(1): p. 33-39.

45. Giroux, E.L. and R.I. Henkin, *Macromolecular ligands of exchangeable copper, zinc and cadmium in human serum.* Bioinorganic Chemistry, 1973. **2**(2): p. 125-133.

46. Mothes, E. and P. Faller, *Evidence that the principal CoII-binding site in human serum albumin is not at the N-terminus: implication on the albumin cobalt binding test for detecting myocardial ischemia.* Biochemistry, 2007. **46**(8): p. 2267-74.

47. Bal, W., et al., *Binding of transition metal ions to albumin: sites, affinities and rates.* Biochim Biophys Acta, 2013. **1830**(12): p. 5444-55.

48. Sokolowska, M., et al., *Short peptides are not reliable models of thermodynamic and kinetic properties of the N-terminal metal binding site in serum albumin.* European Journal of Biochemistry, 2002. **269**(4): p. 1323-1331.

49. Babson, A.L. and T. Winnick, *Protein Transfer in Tumor-bearing Rats.* Cancer Research, 1954. **14**(8): p. 606-611.

50. Kratz, F. and U. Beyer, *Serum Proteins as Drug Carriers of Anticancer Agents: A Review.* Drug Delivery, 1998. **5**(4): p. 281-299.

51. Williams, J. and K. Moreton, *The distribution of iron between the metal-binding sites of transferrin human serum.* Biochemical Journal, 1980. **185**(2): p. 483-488.

52. Dhungana, S., et al., *Redox properties of human transferrin bound to its receptor.* Biochemistry, 2004. **43**(1): p. 205-9.

53. Ohgami, R.S., et al., *Identification of a ferrireductase required for efficient transferrin-dependent iron uptake in erythroid cells.* Nature Genetics, 2005. **37**(11): p. 1264-1269.

54. Steere, A.N., et al., *Kinetics of iron release from transferrin bound to the transferrin receptor at endosomal pH.* Biochimica et Biophysica Acta - General Subjects, 2012. **1820**(3): p. 326-333.

55. Sun, H., H. Li, and P.J. Sadler, *Transferrin as a metal ion mediator.* Chemical Reviews, 1999. **99**(9): p. 2817-2842.

56. Spik, G., et al., *Studies on glycoconjugates. LXIV. Complete structure of two carbohydrate units of human serotransferrin.* FEBS Letters, 1975. **50**(3): p. 296-299.

57. Satomi, Y., Y. Shimonishi, and T. Takao, *N-glycosylation at Asn491 in the Asn-Xaa-Cys motif of human transferrin.* FEBS Letters, 2004. **576**(1–2): p. 51-56.

58. Satomi, Y., et al., *Site-specific carbohydrate profiling of human transferrin by nano-flow liquid chromatography/electrospray ionization mass spectrometry.* Rapid Communications in Mass Spectrometry, 2004. **18**(24): p. 2983-2988.

59. Muchmore, E.A., S. Diaz, and A. Varki, *A structural difference between the cell surfaces of humans and the great apes.* American Journal of Physical Anthropology, 1998. **107**(2): p. 187-198.

60. Oda, R.P., et al., *Capillary electrophoresis-based separation of transferrin sialoforms in patients with carbohydrate-deficient glycoprotein syndrome.* ELECTROPHORESIS, 1997. **18**(10): p. 1819-1826.

61. Golka, K. and A. Wiese, *CARBOHYDRATE-DEFICIENT TRANSFERRIN (CDT)—A BIOMARKER FOR LONG-TERM ALCOHOL CONSUMPTION.* Journal of Toxicology and Environmental Health, Part B, 2004. **7**(4): p. 319-337.

62. Guntiñas, M.B., G. Bordin, and A.R. Rodriguez, *Study of the feasibility of using a pellicular anion-exchange column for separation of transferrin isoforms in human serum by HPLC with UV detection.* Analytical and Bioanalytical Chemistry, 2004. **378**(2): p. 383-387.

63.   Mason, A.B., et al., *Expression of glycosylated and nonglycosylated human transferrin in mammalian cells. Characterization of the recombinant proteins with comparison to three commercially available transferrins.* Biochemistry, 1993. **32**(20): p. 5472-5479.

64.   Mason, A.B., et al., *Differential Effect of a His Tag at the N- and C-Termini: Functional Studies with Recombinant Human Serum Transferrin†.* Biochemistry, 2002. **41**(30): p. 9448-9454.

65.   Hoefkens, P., et al., *Influence of transferrin glycans on receptor binding and iron-donation.* Glycoconjugate Journal, 1997. **14**(2): p. 289-295.

66.   Spik, G., et al., *Primary and Three-Dimensional Structure of Lactotransferrin (Lactoferrin) Glycans*, in *Lactoferrin*, T.W. Hutchens, S. Rumball, and B. Lönnerdal, Editors. 1994, Springer US. p. 21-32.

67.   Ritchie, R.F., et al., *Reference distributions for the negative acute-phase serum proteins, albumin, transferrin and transthyretin: a practical, simple and clinically relevant approach in a large cohort.* Journal of clinical laboratory analysis, 1999. **13**(6): p. 273-279.

68.   Ahmed, N., et al., *Proteomic tracking of serum protein isoforms as screening biomarkers of ovarian cancer.* PROTEOMICS, 2005. **5**(17): p. 4625-4636.

69.   Tosner, J., J. Krejsek, and B. Louda, *Serum prealbumin, transferrin and alpha-1-acid glycoprotein in patients with gynecological carcinomas.* Neoplasma, 1987. **35**(4): p. 403-411.

70.   Saldova, R., et al., *Glycosylation changes on serum glycoproteins in ovarian cancer may contribute to disease pathogenesis.* Disease Markers, 2008. **25**(4): p. 219-232.

71.   Dube, D.H. and C.R. Bertozzi, *Glycans in cancer and inflammation - potential for therapeutics and diagnostics.* Nature Reviews Drug Discovery, 2005. **4**(6): p. 477-488.

72.   Kim, Y. and A. Varki, *Perspectives on the significance of altered glycosylation of glycoproteins in cancer.* Glycoconjugate Journal, 1997. **14**(5): p. 569-576.

73.   Yamashita, K., et al., *Altered glycosylation of serum transferrin of patients with hepatocellular carcinoma.* Journal of Biological Chemistry, 1989. **264**(5): p. 2415-2423.

74.   Daniels, T.R., et al., *The transferrin receptor and the targeted delivery of therapeutic agents against cancer.* Biochimica et Biophysica Acta - General Subjects, 2012. **1820**(3): p. 291-317.

75.   Cox, M.C., et al., *Identification of platination sites on human serum transferrin using 13C and 15N NMR spectroscopy.* Journal of Biological Inorganic Chemistry, 1999. **4**(5): p. 621-631.

76.   Allardyce, C.S., et al., *Determination of drug binding sites to proteins by electrospray ionisation mass spectrometry: the interaction of cisplatin with transferrin.* Rapid Communications in Mass Spectrometry, 2002. **16**(10): p. 933-935.

77.   Dovichi, N.J. and J. Zhang, *How Capillary Electrophoresis Sequenced the Human Genome.* Angewandte Chemie International Edition, 2000. **39**(24): p. 4463-4468.

78.   Lauer, H.H. and G.P. Rozing, *High Performance Capillary Electrophoresis - A Primer.*2010: Agilent Technologies.

79.   Hiemenz, P.C. and R. Rajagopalan, *Principles of Colloid and Surface Chemistry, revised and expanded*. Vol. 14. 1997: CRC Press.

80.   VanOrman, B.B., et al., *Effects of buffer composition on electroosmotic flow in capillary electrophoresis.* Journal of Microcolumn Separations, 1990. **2**(4): p. 176-180.

81.   Whatley, H., *Basic Principles and Modes of Capillary Electrophoresis*, in *Clinical and Forensic Applications of Capillary Electrophoresis*, J. Petersen and A. Mohammad, Editors. 2001, Humana Press. p. 21-58.

82.   Bonvin, G., S. Rudaz, and J. Schappler, *In-spray supercharging of intact proteins by CE-ESI-MS using sheath liquid interface.* Analytica Chimica Acta, 2014. **813**: p. 97-105.

83.   Stutz, H., *Protein attachment onto silica surfaces – a survey of molecular fundamentals, resulting effects and novel preventive strategies in CE.* ELECTROPHORESIS, 2009. **30**(12): p. 2032-2061.

84.   Huhn, C., et al., *Relevance and use of capillary coatings in capillary electrophoresis–mass spectrometry.* Analytical and Bioanalytical Chemistry, 2010. **396**(1): p. 297-314.

85.   Lucy, C.A., A.M. MacDonald, and M.D. Gulcev, *Non-covalent capillary coatings for protein separations in capillary electrophoresis.* Journal of Chromatography A, 2008. **1184**(1–2): p. 81-105.

86.   Tran, N.T., et al., *Poly(ethylene oxide) facilitates the characterization of an affinity between strongly basic proteins with DNA by affinity capillary electrophoresis.* ELECTROPHORESIS, 2005. **26**(16): p. 3105-3112.

87.   Iki, N. and E.S. Yeung, *Non-bonded poly(ethylene oxide) polymer-coated column for protein separation by capillary electrophoresis.* Journal of Chromatography A, 1996. **731**(1–2): p. 273-282.

88.   Gilges, M., M.H. Kleemiss, and G. Schomburg, *Capillary Zone Electrophoresis Separations of Basic and Acidic Proteins Using Poly(vinyl alcohol) Coatings in Fused Silica Capillaries.* Analytical Chemistry, 1994. **66**(13): p. 2038-2046.

89.   Ng, C.L., H.K. Lee, and S.F.Y. Li, *Prevention of protein adsorption on surfaces by polyethylene oxide-polypropylene oxide-polyethylene oxide triblock copolymers in capillary electrophoresis.* Journal of Chromatography A, 1994. **659**(2): p. 427-434.

90.   Belder, D., et al., *Cross-linked poly(vinyl alcohol) as permanent hydrophilic column coating for capillary electrophoresis.* ELECTROPHORESIS, 2001. **22**(17): p. 3813-3818.

91.   Chiari, M., M. Cretich, and J. Horvath, *A new absorbed coating for DNA fragment analysis by capillary electrophoresis.* ELECTROPHORESIS, 2000. **21**(8): p. 1521-1526.

92.   Cretich, M., et al., *Decreased protein peak asymmetry and width due to static capillary coating with hydrophilic derivatives of polydimethylacrylamide.* ELECTROPHORESIS, 2002. **23**(14): p. 2274-2278.

93. Albarghouthi, M.N., T.M. Stein, and A.E. Barron, *Poly-N-hydroxyethylacrylamide as a novel, adsorbed coating for protein separation by capillary electrophoresis.* ELECTROPHORESIS, 2003. **24**(7-8): p. 1166-1175.

94. Simó, C., et al., *Capillary electrophoresis-mass spectrometry of basic proteins using a new physically adsorbed polymer coating. Some applications in food analysis.* ELECTROPHORESIS, 2004. **25**(13): p. 2056-2064.

95. Bernal, J., et al., *Fast and easy coating for capillary electrophoresis based on a physically adsorbed cationic copolymer.* Journal of Chromatography A, 2008. **1204**(1): p. 104-109.

96. Shou, C.-Q., et al., *Preparation and evaluation of non-bonded hyperbranched polymer-coated columns for capillary electrophoresis.* Talanta, 2004. **63**(4): p. 887-891.

97. Shen, Y. and R.D. Smith, *High-resolution capillary isoelectric focusing of proteins using highly hydrophilic-substituted cellulose-coated capillaries.* Journal of Microcolumn Separations, 2000. **12**(3): p. 135-141.

98. Katayama, H., Y. Ishihama, and N. Asakawa, *Stable Capillary Coating with Successive Multiple Ionic Polymer Layers.* Analytical Chemistry, 1998. **70**(11): p. 2254-2260.

99. Mizzen, C.A. and D.R. McLachlan, *Capillary electrophoresis of histone H1 variants at neutral pH in dynamically modified fused- silica tubing.* ELECTROPHORESIS, 2000. **21**(12): p. 2359-2367.

100. Lin, C.-Y., et al., *Simultaneous separation of anionic and cationic proteins by capillary electrophoresis using high concentration of poly(diallyldimethylammonium chloride) as an additive.* Journal of Chromatography A, 2007. **1165**(1–2): p. 219-225.

101. Hardenborg, E., et al., *Novel polyamine coating providing non-covalent deactivation and reversed electroosmotic flow of fused-silica capillaries for capillary electrophoresis.* Journal of Chromatography A, 2003. **1003**(1–2): p. 217-221.

102. Ullsten, S., et al., *A polyamine coating for enhanced capillary electrophoresis-electrospray ionization-mass spectrometry of proteins and peptides.* ELECTROPHORESIS, 2004. **25**(13): p. 2090-2099.

103. Huang, X., Q. Wang, and B. Huang, *Preparation and evaluation of stable coating for capillary electrophoresis using coupled chitosan as coated modifier.* Talanta, 2006. **69**(2): p. 463-468.

104. Katayama, H., Y. Ishihama, and N. Asakawa, *Stable Cationic Capillary Coating with Successive Multiple Ionic Polymer Layers for Capillary Electrophoresis.* Analytical Chemistry, 1998. **70**(24): p. 5272-5277.

105. Nehmé, R., et al., *Influence of polyelectrolyte coating conditions on capillary coating stability and separation efficiency in capillary electrophoresis.* ELECTROPHORESIS, 2008. **29**(14): p. 3013-3023.

106. Bendahl, L., S.H. Hansen, and B. Gammelgaard, *Capillaries modified by noncovalent anionic polymer adsorption for capillary zone electrophoresis, micellar electrokinetic capillary chromatography and capillary electrophoresis mass spectrometry.* ELECTROPHORESIS, 2001. **22**(12): p. 2565-2573.

107.   Catai, J.R., et al., *Analysis of recombinant human growth hormone by capillary electrophoresis with bilayer-coated capillaries using UV and MS detection.* Journal of Chromatography B, 2007. **852**(1–2): p. 160-166.

108.   Janssens, J., R. Chevigne, and P. Louis, *Rinsing a capillary with an initiator, adding buffers then sample and performing electrophoresis*, 1997, United States Patent.

109.   Ciccone, B., *A buffer system for capillary electrophoresis.* American laboratory, 2001. **33**(14): p. 30-33.

110.   Joneli, J., C. Lanz, and W. Thormann, *Capillary zone electrophoresis determination of carbohydrate-deficient transferrin using the new CEofix reagents under high-resolution conditions.* Journal of Chromatography A, 2006. **1130**(2): p. 272-280.

111.   Klampfl, C.W., *CE with MS detection: A rapidly developing hyphenated technique.* ELECTROPHORESIS, 2009. **30**(S1): p. S83-S91.

112.   Denton, K.A. and R. Harris, *High-performance capillary electrophoretic separation of human serum albumin using a neutral coated capillary.* Journal of Chromatography A, 1995. **705**(2): p. 335-341.

113.   Girard, M., H.P. Bietlot, and T.D. Cyr, *Characterisation of human serum albumin heterogeneity by capillary zone electrophoresis and electrospray ionization mass spectrometry.* Journal of Chromatography A, 1997. **772**(1–2): p. 235-242.

114.   Girard, M., et al., *Use of capillary electrophoresis for the characterization of human serum albumin heterogeneity.* Biomedical Chromatography, 1998. **12**(3): p. 183-184.

115.   Alahmad, Y., et al., *A new CZE method for profiling human serum albumin and its related forms to assess the quality of biopharmaceuticals.* ELECTROPHORESIS, 2011. **32**(2): p. 292-299.

116.   Marie, A.L., et al., *Capillary zone electrophoresis and capillary electrophoresis-mass spectrometry for analyzing qualitative and quantitative variations in therapeutic albumin.* Analytica Chimica Acta, 2013. **800**: p. 103-10.

117.   Sanz-Nebot, V., et al., *Characterization of transferrin glycoforms in human serum by CE-UV and CE-ESI-MS.* ELECTROPHORESIS, 2007. **28**(12): p. 1949-1957.

118.   Kohler, I., et al., *New insights in carbohydrate-deficient transferrin analysis with capillary electrophoresis–mass spectrometry.* Forensic Science International, 2014. **243**: p. 14-22.

119.   Dhara, S.C., *A rapid method for the synthesis of cis-[PtCl$_2$(NH$_3$)$_2$].* Indian Journal of Chemistry, Section B, 1970(8): p. 193-194.

120.   Nehmé, R. and C. Perrin, *Highly Charged Polyelectrolyte Coatings to Prevent Adsorption During Protein and Peptide Analysis in Capillary Electrophoresis*, in *Capillary Electrophoresis of Biomolecules*, N. Volpi and F. Maccari, Editors. 2013, Humana Press. p. 191-206.

121.   N.N. *UltraTrol^{TM} Dynamic Pre-Coatings User Manual*. 2004 05.05.2014; Available from: http://www.targetdiscovery.com/~tdidocs/UltraTrolUserManRevB.pdf.

122. Towns, J.K. and F.E. Regnier, *Capillary electrophoretic separations of proteins using nonionic surfactant coatings.* Analytical Chemistry, 1991. **63**(11): p. 1126-1132.

123. Espinal, J.H., J.E. Gómez, and J.E. Sandoval, *Closer look at the operating definition of protein recovery in CE.* ELECTROPHORESIS, 2013. **34**(8): p. 1141-1147.

124. Ermakov, S.V., et al., *Wall adsorption in capillary electrophoresis experimental study and computer simulation.* Journal of Chromatography A, 1995. **699**(1–2): p. 297-313.

125. Reedijk, J. and P.H.M. Lohman, *Cisplatin: Synthesis, antitumour activity and mechanism of action.* Pharmaceutisch Weekblad, 1985. **7**(5): p. 173-180.

126. Nagai, N., et al., *Decomposition Kinetics of Cisplatin in Human Biological Fluids.* Journal of Pharmacy and Pharmacology, 1996. **48**(9): p. 918-924.

127. Caslavska, J. and W. Thormann, *Monitoring of alcohol markers by capillary electrophoresis.* Journal of Separation Science, 2013. **36**(1): p. 75-95.

128. Killmann, E., H. Maier, and J.A. Baker, *Hydrodynamic layer thicknesses of various adsorbed polymers on precipitated silica and polystyrene latex.* Colloids and Surfaces, 1988. **31**(0): p. 51-71.

129. Kayes, J.B. and D.A. Rawlins, *Adsorption characteristics of certain polyoxyethylene-polyoxypropylene block co-polymers on polystyrene latex.* Colloid and Polymer Science, 1979. **257**(6): p. 622-629.

130. Tanaka, Y., et al., *Development of a capillary electrophoresis-mass spectrometry method using polymer capillaries for metabolomic analysis of yeast.* ELECTROPHORESIS, 2008. **29**(10): p. 2016-2023.

131. Haselberg, R., G.J. de Jong, and G.W. Somsen, *CE-MS for the analysis of intact proteins 2010–2012.* ELECTROPHORESIS, 2013. **34**(1): p. 99-112.

Curriculum Vitae

Christian Artner, BSc.

E-mail   christian.artner@univie.ac.at

Education

05.2013-now	Master thesis at the University of Vienna in the group of Prof. B.K. Keppler Thesis Title: Investigations of Intact Human Serum Albumin and Transferrin Isoforms Interacting with Anticancer Metallodrugs by Capillary Electrophoresis
2011-now	Master´s programme in chemistry at the University of Vienna
11.2011	Bachelor´s degree in chemistry Thesis Title: Synthese und Charakterisierung tumorhemmender Platin(IV) Komplexe
03.2006	Begin of studies in chemistry and biology at the University of Vienna
06.2005	Matura
1997-2005	Bundesrealgymnasium Mattersburg
1993-1997	Volksschule Wiesen

Research interests

analytical, biological and inorganic chemistry

drug development, separation techniques

capillary electrophoresis, mass spectrometry

Relevant working experience

07.2009   Summer   internship: Murexin   AG,
                                           investigations of elemental composition of
                                           building materials by X-ray fluorescence
                                           spectroscopy

Languages

German (native tongue)

English

French (basics)

Driver License

B, C, F

Ich habe mich bemüht, sämtliche Inhaber der Bildrechte ausfindig zu machen und ihre Zustimmung zur Verwendung der Bilder in dieser Arbeit eingeholt. Sollte dennoch eine Urheberrechtsverletzung bekannt werden, ersuche ich um Meldung bei mir.   C.A.